IS-T--1480

DE90 011737

Spectral Hole Burning Studies of Photosystem I

by

J. Kevin Gillie

PHD Thesis submitted to Iowa State University

Ames Laboratory, U.S. DOE

Iowa State University

Ames, Iowa 50011

Date Transmitted: January 1990

PREPARED FOR THE U. S. DEPARTMENT OF ENERGY

UNDER CONTRACT NO. W-7405-Eng-82.

1480

Spectral hole burning studies of Photosystem I

J. Kevin Gillie

Under the supervision of Gerald J. Small
From the Department of Chemistry
Iowa State University

Persistent spectral hole burning is applied to the reaction center, P700, and the light harvesting chlorophyll protein complexes of Photosystem I. A theory for solid state spectral hole burning is developed that is valid for arbitrarily strong linear electron-phonon coupling within the Condon approximation. Persistent photochemical hole burning of the reaction center P700, reveals that a broad (~300 cm^{-1}) hole can be burned into the absorption profile. The hole profile and its maximum position and intensity dependence on burn wavelength are adequately fit by the electron-phonon coupling theory. The results indicate that the absorption and hole profile are dominated by phonon transitions with a Huang-Rhys factor of ~8. A dimer structure for P700 is supported. The similarities to the primary electron donor states of other reaction centers are examined.

Nonphotochemical hole burning spectra for the Q_y transitions associated with the light harvesting antenna complex of Photosystem I are presented. The frequencies and Franck-Condon factors are determined for 41 chlorophyll a and 12 chlorophyll b intramolecular modes. The linear electron-vibration coupling for all modes is very weak with the maximum Franck-Condon factor observed being ~0.04. The linear electron-phonon coupling for protein modes of mean frequency

22 cm^{-1} is weak with Huang-Rhys factor of 0.8. The electron-phonon coupling of the antenna system is compared with that for P700. The intramolecular modes, phonon frequencies, and Franck-Condon factors are used with multiphonon excitation transport theories to analyze the available temperature-dependent data on the kinetics of transport within the core antenna complex. Phonons (not intramolecular modes) mediate excitation transport within the antenna and from antenna to reaction center. The results also indicate that a subunit or cluster model for the antenna provide a more accurate picture than the regular array model for excitation transport.

Spectral hole burning studies of Photosystem 1

by

J. Kevin Gillie

A Dissertation Submitted to the

Graduate Faculty in Partial Fulfillment of the

Requirements for the Degree of

DOCTOR OF PHILOSOPHY

Department: Chemistry
Major: Physical Chemistry

Approved:

Gerald J. Small
In Charge of Major Work

For the Major Department

For the Graduate College

Iowa State University
Ames, Iowa

1989

TABLE OF CONTENTS

reprints removed. ds

reprints removed ds

EXPLANATION OF DISSERTATION FORMAT

This dissertation contains the candidate's original work on spectral hole burning of Photosystem I. Section I contains two published papers which describe a linear electron-phonon coupling theory that was developed to model the spectral properties of the primary electron donor states of photosynthetic systems and application of the theory to P700 of Photosystem I. Section II contains two published papers which report hole burning experiments performed on the light harvesting chlorophyll complex of Photosystem I and application of multiphonon excitation energy transport theory to these results. Each section contains an introduction, two papers, and additional results. The references for the introduction and additional results of each section are located at the end of that section. The references for each paper are found at the end of that paper.

GENERAL INTRODUCTION

Photosynthesis is one of the many fascinating biophysical energy conversion processes that occur in nature. It is unique, however, since the energy source for the basic photosynthetic equation

$$CO_2 + H_2O + 478\ kJ \rightarrow [CH_2O] + O_2$$

is sunlight. That is, photosynthesis utilizes solar energy to reduce carbon dioxide to carbohydrates. One einstein (one mole of photons) at 680 nm contains only ~ 175 kJ. It is recognized then, that nature had to construct sophisticated systems to collect and convert solar energy. The first evidence for such systems was provided by Emerson and Arnold [1] when they demonstrated that large numbers of chlorophylls (Chl) cooperated to produce oxygen via photosynthesis. Although the basic photosynthesis equation is simple, the processes occurring in the thylakoid membranes are complicated. The primary events of light harvesting and charge separation are the concern of this work.

The thylakoid membrane of green plant chloroplast contains hundreds of protein bound pigments arranged into two functional groups: i) the reaction centers and ii) the light harvesting complexes. The physical organization of the thylakoid membranes has been extensively reviewed [2 and refs. therein] and is shown in Fig. 1. The thylakoid membrane consist of two photosynthetic units (PSU), Photosystem I (PSI) and Photosystem II (PSII), which function cooperatively in photosynthesis. The reaction centers (RC) are labeled P700 (for PSI) and P680 (for PSII) to indicate the position, 700 nm and 680 nm, of the maximum of the light induced absorption decrease.

The light harvesting chlorophyll protein complexes (LHCI and LHCII) contain

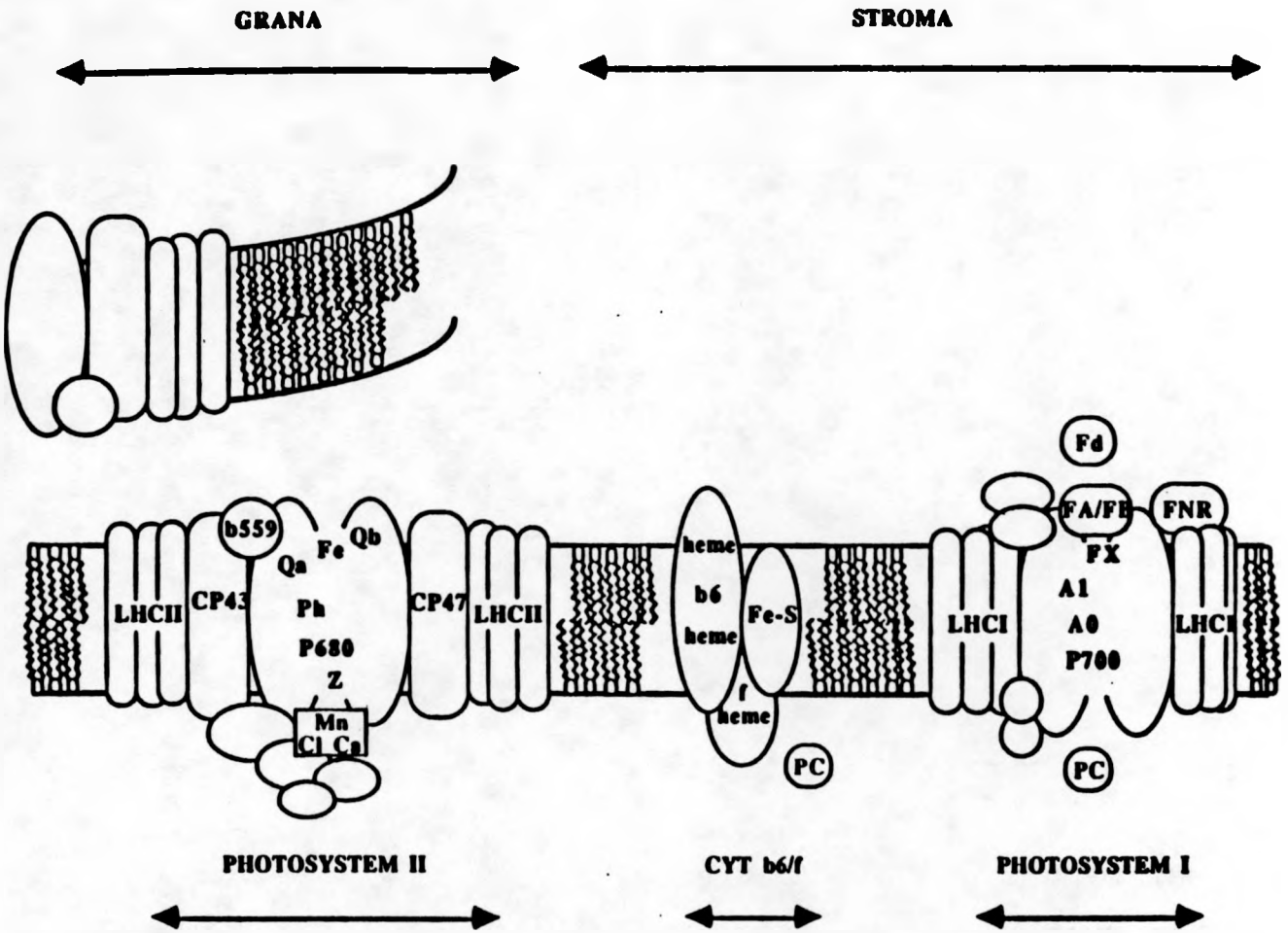

Figure 1. The physical organization of the Photosystem I, cytochrome b6/f, and Photosystem II protein complexes within the thylakoid membrane. The cyt b6/f complex transfers an e^- from PSII to PSI via plastocyanine (PC) (reprinted from ref. 3).

protein bound chlorophyll a (Chl a) and chlorophyll b (Chl b). These protein complexes and the core Chl a protein complexes serve the RCs as antenna complexes to collect and transfer solar energy to the RC. For PSI, there are about 200 Chls per reaction center. The antenna complexes serve to increase the amount of the solar spectrum that is employed by broadening the photosystem's absorption (different spectral forms of Chls) [4-7] and by increasing the absorptivity (additive in number of molecules) over the isolated RC absorption profile.

Since the quantum yield for photosynthesis is ~1 [8], it is interesting to consider how energy can be transferred over large spatial distances in the antenna in a manner that competes successfully with other radiative and non-radiative decay channels. The orientation of the proteins with respect to the RC, the organization of the Chls within the proteins, the dynamical role of the proteins and the electronic states of the Chls are important components of any answer to this question.

The energy delivered by the antenna complex is photoconverted at the RC to a stabilized charge separation. In PSII, excitation of the primary electron donor (PED), P680, leads to electron transfer to a pheophytin (Pheo) acceptor [9-11] and subsequent transfer to a quinone where the charge is stabilized [12]. The P680 $\rightarrow$ Pheo e^- transfer occurs in ~3 psec [13,14]. The charge separation in PSI occurs within ~3 psec [15] at room temperature with production of the charge separated state $P700^+A_0^-$ (A_0 is the primary acceptor) within ~14 psec [16]. Overall, the RCs produce an energy change of 1.22V.

The e^- necessary for reducing $P680^+$ is provided by splitting H_2O. Eight photons are required to produce one molecule of oxygen. The e^- produced in charge stabilized P680 reaction center is passed into the cytochrome b6/f (cyt b_6/f) complex where it is ultimately used to reduced $P700^+$. This process translocates a proton

across the membrane thereby producing a pH and electric field gradient which is used for generating ATP. The electron available from P700 excitation is passed to the ferredoxin (Fd) and reduces $NADP^+$ to NADPH. It is NADPH and ATP which the dark reactions (Calvin cycle) use to reduce CO_2 to carbohydrates. As in the antenna complex, acceptor orientation, protein dynamics, and electronic states play important roles in efficient charge separation and stabilization.

The PSI protein complex is shown schematically in Fig. 2 [see refs. 3,17-20 for reviews]. The structure has not yet been determined by X-ray crystallography so this represents a proposal based on a large volume of biochemical evidence [3,17]. CP1, the P700 chlorophyll a-protein, contains the core antenna complex, active P700 and A_o, and A_1. It is a subset of the core protein which includes, along with CP1, the e^- acceptors A_1 and F_x and the high molecular weight (82 and 83 kDa) polypeptides. The enriched PSI core complex is the smallest fully functional RC particle. It contains P700, the e^- acceptors A_o, A_1, F_x, F_a/F_b and ~7 polypeptides including the core antenna complex. The identity of the acceptors is given in Table I. The PSI core complex is enriched to ~30 Chl a per reaction center. The "native" PSI particle contains, in addition to the core complex, LHCI and is the most physiologically intact particle. The LHCI complex contains ~170 Chl with a Chl a /Chl b ratio of ~6 [21,22]. The overall Chl a/Chl b ratio in PSI-200 is ~3.5 [21,23,24].

A proposed structure for P700 is shown in Fig. 3. It is based on biochemical evidence and reflects the structure determined for the purple photosynthetic bacteria Rhodopseudomonas viridis (Rps. viridis) [25-28] and Rhodobacter sphaeroides (Rb. sphaeroides) [29,30]. It maintains the pseudo-symmetry (C_2) found in the purple bacteria and suggested for PSII. The precise structural arrangement awaits X-ray

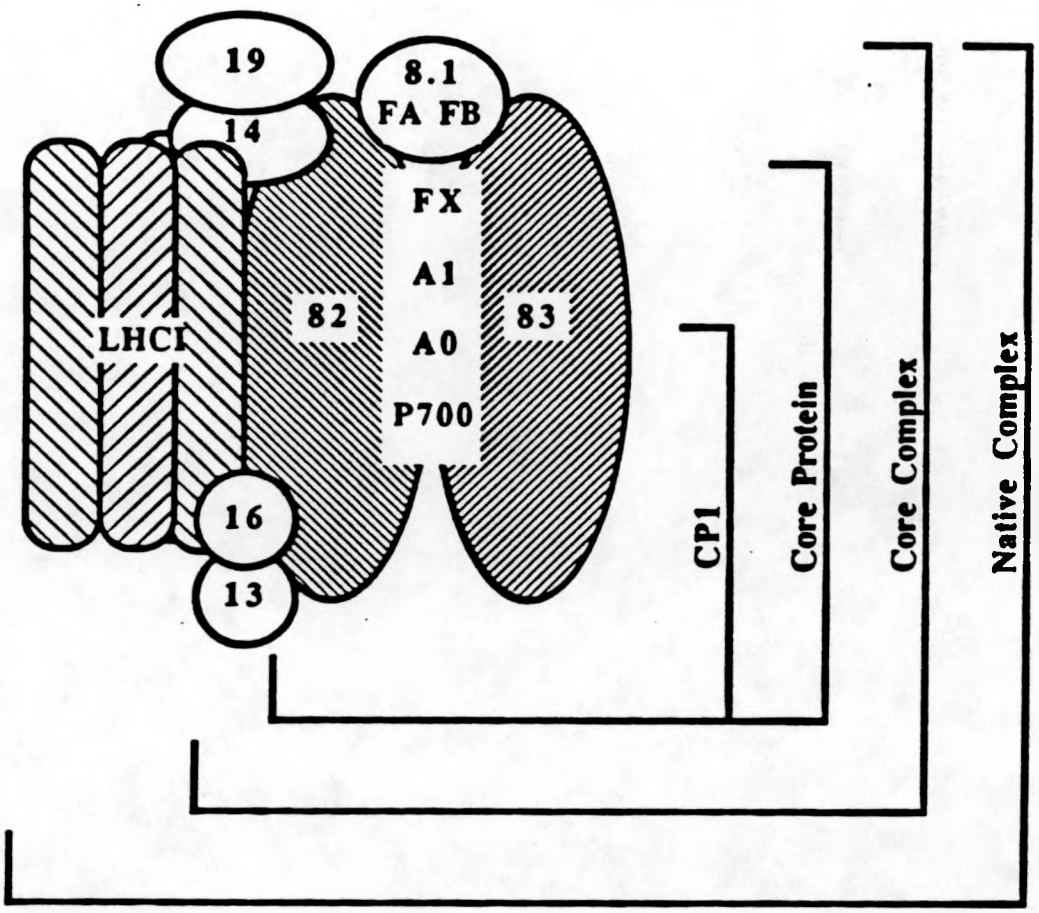

Figure 2. A schematic of the Photosystem I protein complex indicating the polypeptide composition of the isolatable particles. The shaded polypeptides represented chlorophyll-bearing proteins (reprinted from ref. 3).

Table I. Donor/acceptor indentity of the Photosystem I polypeptides

Donor/Acceptor	Identity
P700	Chlorophyll dimer
A_o	Chlorophyll monomer
A_1	Vitamin K_1
F_x	[XFe - XS]Cluster (X=2,4)
F_B	[4Fe - 4S]Cluster
F_A	[4Fe - 4S]Cluster
F_D	Ferredoxin
FNR	Ferredoxin:$NADP^+$oxidoreductase

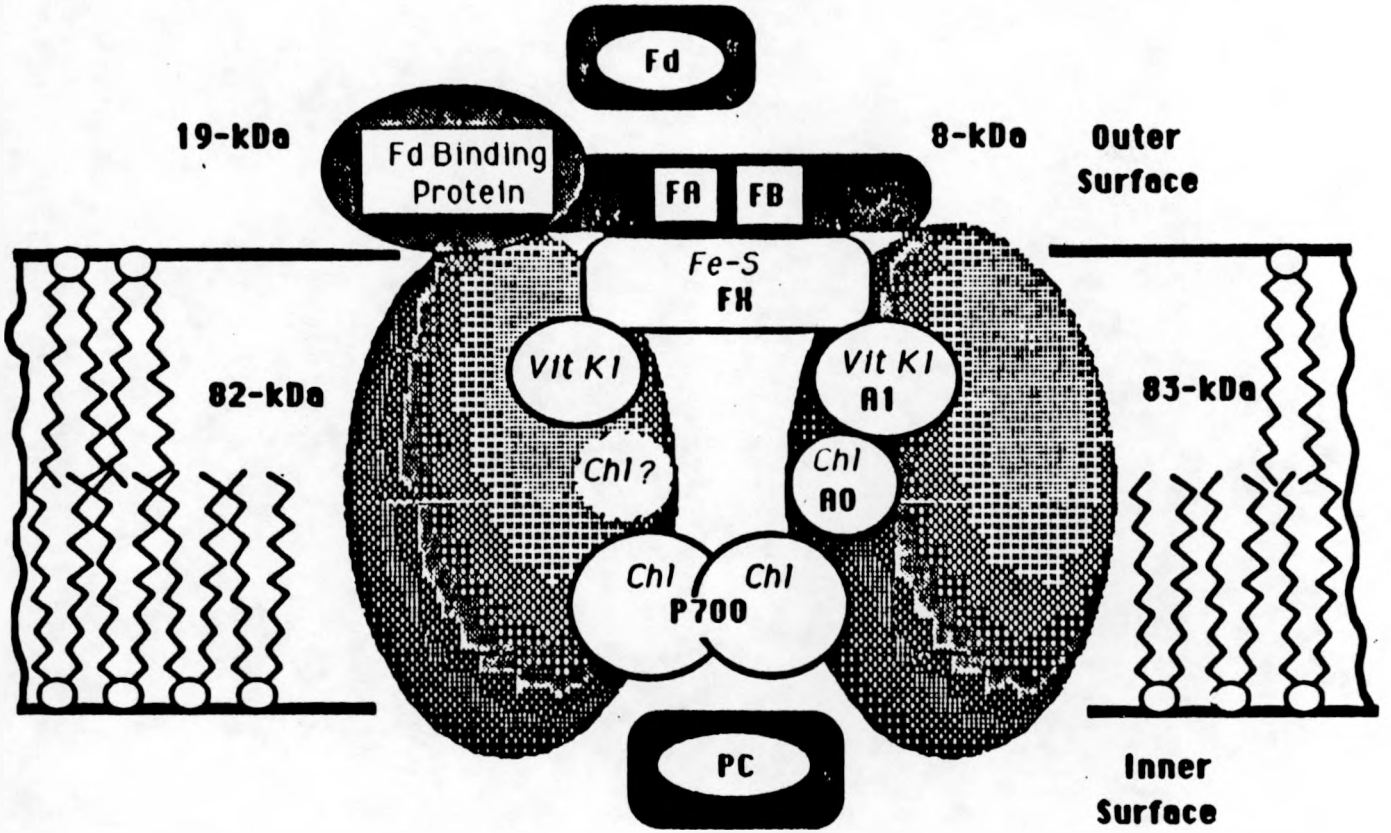

Figure 3. A proposed structure for the Photosystem I reaction center. It reflects biochemical evidence and the structure determined for the reaction center of purple photosynthetic bacteria (reprinted from ref. 3).

structure analysis of the recently crystallized PSI complex from cyanobacteria [31,32].

The absorption spectrum of PSI at room temperature is shown in Fig. 4. The dominant absorption feature is the lowest excited singlet state ($S_1 \leftarrow S_0$) transition, the Q_y transition, of the protein bound Chl a antenna complex at 670 nm. The Q_y transition for Chl b is at 650 nm. The $S_2 \leftarrow S_0$ or Q_x transition lies at about 575 nm for Chl a. The primary electron donor state, P700, has its maximum absorption at ~700 nm, a shift of ~750 cm^{-1} from monomer Chl a. To a first approximation, the shift is a result of excitonic interactions between pigment pairs. The carotenoids associated with PSI absorb in the 450-500 nm range and the Chl $S_3 \leftarrow S_0$ and higher transitions, the Soret transitions, lie at <450 nm.

The absorption spectrum sharpens only slightly in cooling the sample to 4.2 K, and it is still dominated by the broad (350 cm^{-1} width) profile of the Chl a Q_y transition. At this temperature it is possible to distinguish the Chl b absorption at 650 nm and the P700 absorption (in enriched particles). The broad profile hides important information - homogeneous linewidths, intramolecular vibrational frequencies, and low energy lattice vibration (phonon) frequencies - about the excited state of the system. The broad low temperature absorption character is similar to that observed for molecules doped into amorphous (glassy) materials. In this case, site selective spectroscopies, spectral hole burning and fluorescence line narrowing, are employed to "trick" the system into mimicking a perfect crystal.

Molecules doped into amorphous materials, e.g., ionic dyes in organic glasses, exhibit a broad absorption spectrum (typically several hundred cm^{-1}) even after cooling to near 0 K. In contrast, molecules doped into perfect crystals exhibit sharp absorption lines (typically <1 cm^{-1}) which correspond to the various electronic

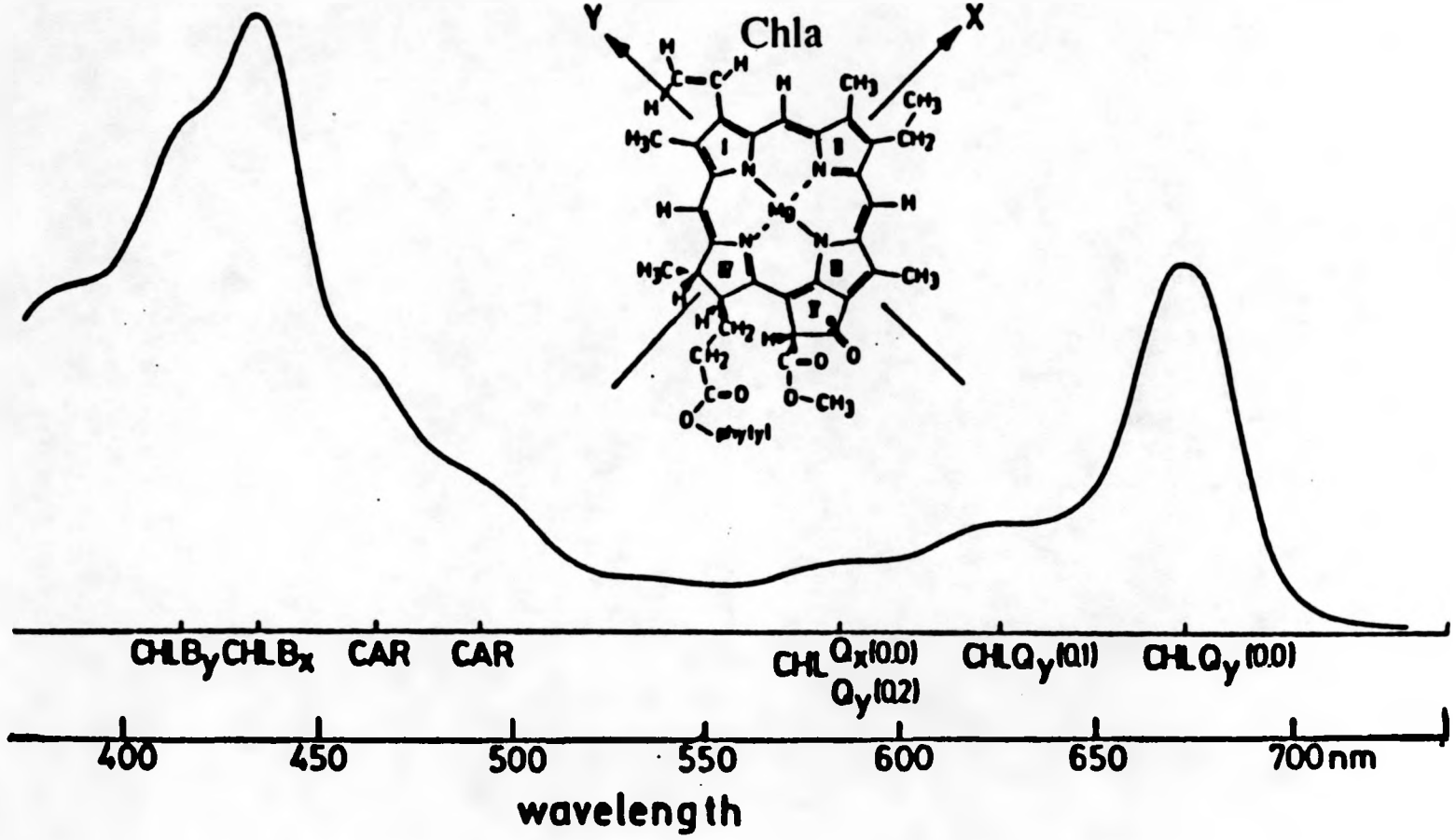

Figure 4. The room temperature absorption spectrum of PSI. The inset shows the conventional axis assignment for Chl a.

(vibronic) transitions of the molecule. The different behaviors are a result of the impurity's microenvironment. For a perfect crystal each impurity molecule has the same environmental interactions and hence the electronic transitions overlap producing the observed homogeneously broadened lines. One important characteristic of amorphous materials is the variation in microscopic site-impurity interactions. Each impurity molecule experiences slightly different environmental interactions which cause the electronic transitions to be distributed around a center frequency. The resulting spectrum is said to be inhomogeneously broadened and consist of the convolution of the homogeneously broadened absorption profile of the individual impurity molecule. This is illustrated in Fig. 5a.

Site selection spectroscopies utilize narrow band (preferably less than the homogeneous linewidth) light sources such as lasers to select a narrow energy window (isochromat) for excitation. The number of molecules excited represents just a small fraction of the total number of molecules in the system and the resulting spectral features are narrow mimicking that of a perfect crystal. The inhomogeniety has been circumvented.

An impurity molecule in a glass can undergo two types of transformations, one photochemical the other photophysical, while in its excited state. In either case, the dopant loses memory of its initial state which results in a depletion of the number of absorbers coincident with the the excitation frequency. This is manifested by a dip or "hole" in the impurity's absorption spectrum, hence the term spectral hole burning. As long as the sample is kept cold (near 0 K), the spectral holes are persistent (transient hole burning via a population bottleneck is also possible). There are two processes that result in spectral holes. Photochemical hole burning, as the name implies, occurs in systems that undergo photochemistry, e.g., proton

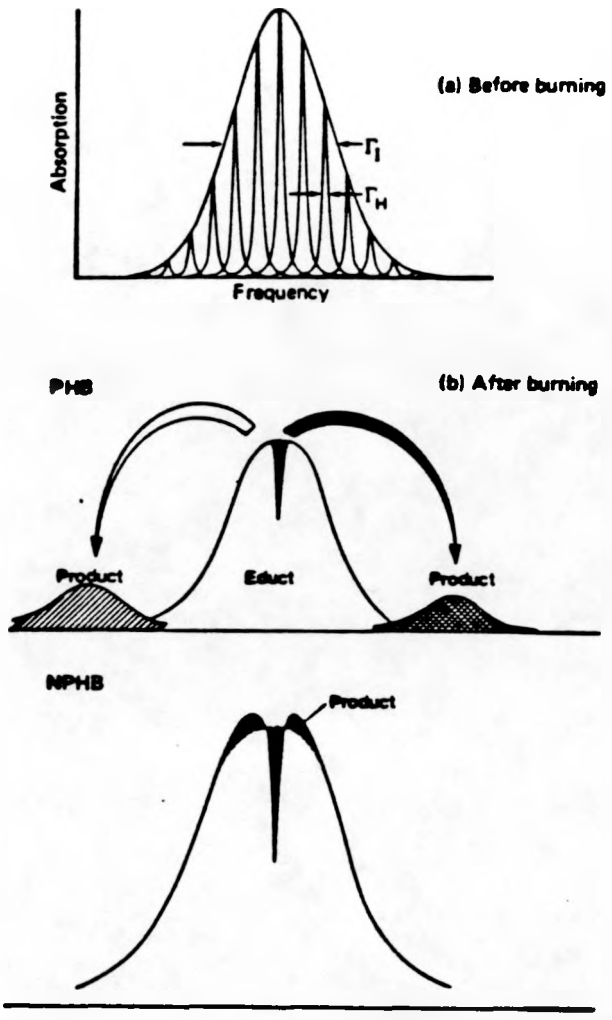

Figure 5. The inhomogeneously broadened absorption spectrum (a)of an impurity in a glass- Γ_h (homogeneous line width)< 1 cm^{-1}; Γ_{inh} (inhomogeneous line width) ~a few hundred cm^{-1} for organic molecules in glasses. The absorption profile after (b) photochemical hole burning and (c) nonphotochemical hole burning.

tautomerization of H_2-phthalocyanine during irradiation with a laser [33]. As shown in Fig. 5b the products from photochemical hole burning (PHB) typically absorb several hundred cm^{-1} away from the spectral hole. Nonphotochemical hole burning is a result of host configuration changes that occur while the impurity is in its excited state. The host-impurity interaction changes are small so typically the anti-hole (product absorption) is displaced $<100\ cm^{-1}$ from the spectral hole, Fig. 5c. Hayes and Small [34,35] proposed that the mechanism for nonphotochemical hole production is phonon assisted tunneling between the glassy states two level systems. Two level systems had already been proposed to explain other glassy state anomalous behavior [36,37].

The spectral linewidth of the hole is related to the time domain by the equation $T_2=(\pi\,\Delta\nu_h)^{-1}$ where T_2, the total dephasing time, is given by $1/T_2= 1/2T_1 + 1/T_2^*$. T_1 processes are those that lead to depopulation of initially prepared excited states and include fluorescence, intersystem crossing, and internal conversion. When a system of molecules is irradiated with a coherent source, they begin to oscillate in phase with themselves and with the radiation field. When the coherent source is removed, the molecules, through their interactions with low energy lattice phonons, begin to lose phase coherence. This process is termed pure dephasing and has a characteristic lifetime T_2^*. T_1 processes occur even at 0 K whereas pure dephasing processes should cease at 0 K. Because of the frequency-time domain relation interesting glassy state properties, e.g. spectral diffusion and dephasing, can be probed with spectral hole burning. A large number of different impurities and host matrices have been shown to produce spectral holes. The science and application of hole burning has been extensively discussed [35,38-40]. Of particular interest here is spectral hole burning of biological pigments hosted in their natural proteins.

Phonons resulting from the displacement of the excited nuclear coordinates of the impurity, relative to its ground state, induce low energy lattice distortions. The strength of the coupling of the excited state potential to the lattice is measured by the Huang-Rhys factor defined as

$$S=\frac{1}{2}\Delta^2$$

where Δ is the displacement of the normal coordinates. The phonon transitions build on the "pure" zero-phonon transition and are reflected in the absorption profile as broad bands at higher energy, relative to the zero-phonon transition, by a mean phonon frequency (typically 10-50 cm^{-1}). The relative intensities of the r-phonon process is given by the Poisson distribution $e^{-S}S^r/r!$ [41 and refs. therein] with S defined as above. For large electron-phonon coupling strengths, the phonon absorption will dominate the spectrum.

The absorption cross-section of the impurity at any particular frequency consist of the overlap of zero-phonon transitions, phonon transitions and vibronic transitions. Spectral hole burning can occur through any of these features. For example, if one chooses a burn frequency on the low energy side of the absorption profile it is possible to produce a zero-phonon hole coincident with the laser. At higher energies in the absorption profile, there is significant overlap of zero-phonon and phonon transitions. A zero-phonon hole coincident with the burn frequency and a pseudo-phonon sideband hole (pseudo-PSBH) to lower energy are produced by irradiation. The pseudo-PSBH is the convolution of zero-phonon transitions that have absorbed radiation through their phonon wings. The mean phonon frequency can be measured from the displacement of the pseudo-PSBH from the zero-phonon

hole. If the sample is irradiated in the congested vibronic regions, vibronic satellite hole structure can be burned into the origin bands. That is, excitation occurs though vibronic transitions and results in the depletion of the number of zero-phonon absorbers in the origin band. The displacement of the satellite holes from the burn frequency gives the excited state vibrational frequencies. By tuning the burn frequency, it is possible to determine all the Franck-Condon active modes.

A number of phenomena affect hole burning. Spectral diffusion and dephasing processes alter the zero-phonon linewidth. The extent to which these processes alter the observed linewidths is much debated [38,39,42-45]. It is an important limitation to the calculation of T_1 lifetimes. Spontaneous hole filling (SPHF) and laser induced hole filling (LIHF) also affect the hole burning. The mechanisms for these phenomena have been investigated for ionic dyes doped in organic glasses [46,47]. Spontaneous hole filling defines the time frame of the hole burning experiment, i.e., one would want to probe the hole before significant hole filling occurs. SPHF has not been observed in the pigment-protein complexes of PSI at 1.6 K.

Application of spectral hole burning to pigment-protein systems is a recent and exciting development. The only requirement is that the pigments absorb in a region accessible to lasers. Probing the primary events of photosynthesis, reaction center and antenna dynamics, with spectral hole burning is the subject of this dissertation.

EXPERIMENTAL METHODS

Samples

The Photosystem I particles with various P700 enrichment levels (actually, antenna chlorophyll depleted) are generously supplied to us by John Golbeck. The particles are prepared following the procedure of Mullet and coworkers [48] and Golbeck [49]. Fragmented thylakoid membranes of spinach chloroplast are obtained by homogenizing leaf spinach with a high speed blender in a buffered (pH 7.8) solution. The freed chloroplast are osmotically shocked, suspended in EDTA to remove loosely bound proteins, and sonicated to produce the fragmented thylakoid membranes. The thylakoid membranes are washed with a non-ionic detergent (Triton X-100) in a buffered solution to produce the "native" PSI-200 particle. Subsequent washing with Triton X-100 results in depletion of the Chl antenna proteins. The Chl to P700 ratio is assayed by photo-oxidizing P700. The extinction coefficient for P700 is ε_{700nm}=64 mM^{-1} cm^{-1}.

The particles, suspended in a buffered glycerol/water mixture (pH 8.0) containing 0.1% Triton X-100, are stored at 77 K until needed. The optical density of the samples was adjusted by dilution to the appropriate value with a buffered (pH 8.3) glycerol/water (70:30) solution containing 100 mM Tris [tris(hydroxymethyl) aminomethane] and 0.1% triton X-100. 1 mM ascorbic acid is added to pre-reduce P700.

The samples were held in the dark for a few minutes before being quickly cooled (< 10 minutes) to 4.2 K. This procedure is required to aid pre-reduction of P700. Subsequent exposure to light is held to a minimum.

Cryogenic Equipment

All liquid samples were placed in a 1 cm diameter polystyrene tube chosen because it minimized sample cracking at low temperatures. The sample tube is held in a brass container of local design which allowed for optical access of the sample. The samples were cooled to 4.2 K in a Janis Model 8-DT Super Vari-Temp liquid Helium cryostat. By pumping with an auxiliary vacuum pump it is possible to take helium past its lambda point (2.25 K) and achieve a temperature of 1.6 K. The sample temperature was monitored using a silicon diode thermometer (Lake Shore Cryogenic model DT-500K) calibrated over the range from 1.4 K to 300 K.

Experimental Apparatus

Figure 6 shows the configuration of the apparatus used for hole burning and subsequent reading. The laser system consist of a 5W argon ion laser (Coherent Innova 90-5) which was used to pump a single frequency passively stabilized ring dye laser (Coherent 699-21). A three plate birefringent filter provides wavelength selection. Narrow laser linewidths (0.002 cm^{-1}) are accomplished with two low finesse intra-cavity etalons having free spectral ranges of 10 GHz and 100 Ghz which combined with the birefringent filter (~380 MHz) forces single longitudinal mode operation. The laser dyes used were DCM and LD688 (Exciton).

The output of the ring laser was monitored for single frequency operation by directing, by means of a beamsplitter, a portion of the laser beam to a confocal spectrum analyzer (Spectra-Physics model 470-40, FSR= 8 GHz). The output of the spectrum analyzer was displayed on an oscilloscope. The laser wavelength was determined by sending a portion of the beam to a 1/3 meter monochromator (McPherson model 218). Laser powers were set using a variable attenuator

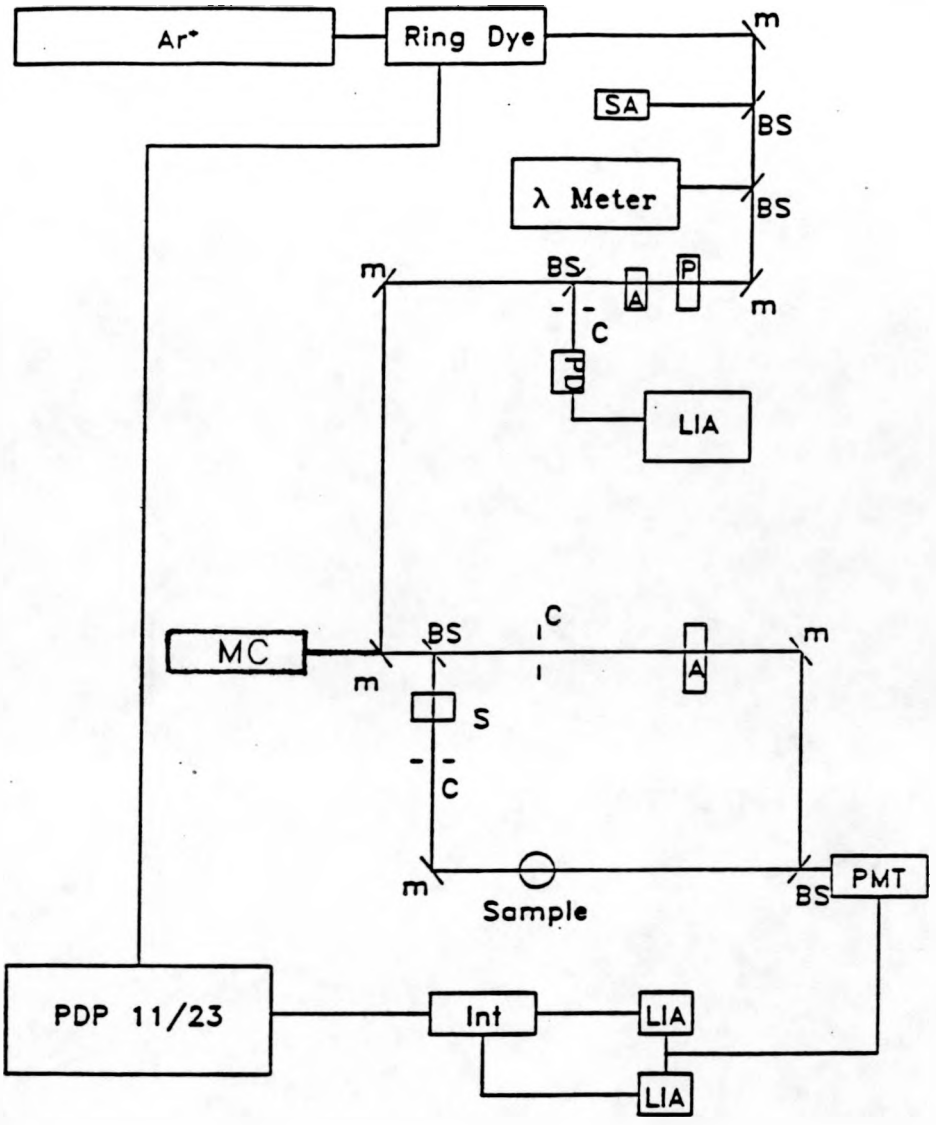

Figure 6. Experimental absorption/hole burning apparatus. Ar^+-argon ion laser; M -mirror; BS -beamsplitter; SA -spectrum analyzer; λmeter wavemeter; P -polarizer; A -attenuator; C -chopper; PD -photodiode; LIA -lock-in amplifier; S -shutter; PMT -photomultiplier tube; INT integrator; MC - monochromator.

(Newport Corporation model 935-3) and neutral density filters. Part of the attenuated beam was extracted, modulated with a mechanical chopper (PAR model 125), and monitored for intensity with a photodiode detector (Molectron 4P-141) and lock-in amplifier (PAR model 124 with a model 118 preamplifier). The laser beam was then directed by mirrors to a home built double beam spectrometer [50,51]. There are two sources available for scanning the holes. The ring dye laser can be scanned through 30 GHz (1 cm^{-1}) by an intra-cavity angle tuned brewster plate. Resolution is 0.002 cm^{-1}. Low resolution (~ 0.2 cm^{-1}) spectra were taken using light from a 500 W short-arc Xenon lamp (Canrad-Hanovia model 959C1980) dispersed by a 1.5 M monochromator (Jobin-Yvon HR1500). The monochromator has a linear dispersion of 0.19 nm/mm (2400 groves/mm grating). Either source could be utilized for hole scanning by retraction of a mirror. In either case, the ring dye laser is employed for burning.

The light incoming onto the double apparatus is split into a reference leg and a sample leg by a beamsplitter. Each leg contains identical optics. The reference leg intensity can be attenuated (Newport Corporation model 925B) to match optical losses on the sample leg caused by scattering from the cryostat and sample. Each leg is modulated at different frequencies with mechanical choppers (Laser Precision CTX-534). The beams are recombined and sent to a cooled photomultiplier tube (RCA C31034 in a PFR PR-1400-RF thermoelectrically cooled housing). The signal is then detected by two lock-in amplifiers (Ithaco model 97EO) referenced to the mechanical choppers. The output from the lock-in amplifiers is integrated (at multiples of 1/60 second) and digitized with an integrator/coupler (Ithaco model 385EO-2) and sent to a microcomputer (Digital Equipment Corporation Micro PDP-11/23+ with RT11 operating system) where it is converted into absorbance and

stored. The computer also drives the scanning of the monochromator and ring dye laser.

Stark Apparatus

The Stark cell was built from polystyrene. A round polystyrene tube was cut to provide a center section about 3 mm thick with parallel sides. Thin polystyrene sheets (0.0015 inches) onto which gold had been vapor deposited were attached to the parallel sides of the tube section with model cement (Testor). Electrical connection is made by means of small screws. The Stark cell is placed in a teflon holder with optical and electrical access and provides electrical insulation. The holder is attached to a sample rod and lowered into the cryostat. DC voltage is supplied by a high voltage supply (Sorenson 1030-20) and measured using a high voltage probe (Fluke 80F-15).

REFERENCES

1. Emerson, R.; Arnold, W. J. Gen. Physiol. 1932, 15, 391; J. Gen Physiol. 1932, 16, 191.

2. Staehelin, L. A. In Photosynthesis III: Photosynthetic Membranes and Light Harvesting Systems; Staehelin, L. A., Arntzen, C. J., Eds.; Springer-Verlag: Berlin, 19, p 1.

3. Golbeck, J. H. Biochim. Biophys. Acta 1987, 895, 167.

4. Seely, G. R. J. Theor. Biology 1973, 40, 173.

5. Glazer, A. N. Annu. Rev. Biochem. 1983, 52, 125.

6. Davis, R. C.; Ditson, S. L.; Fentiman, A. F.; Pearlstein, R. M. J. Amer. Chem. Soc. 1981, 103, 6823.

7. Maggoria, L. L.; Maggoria, G. M. Photochem. Photobiol. 1984, 39, 847.

8. Lien, S.; San Pietro, A. In An Inquiry into Biophotolysis of Water to Produce Hydrogen; a report sponsored by NSF under RANN Grant G140253, 1976.

9. Nuijis, A. M.; van Gorkom, H. J.; Plijter, J. J.; Duysens, L. N. M. Biochim. Biophys. Acta 1986, 848, 167.

10. van Gorkom, H. J.; Nuijis, A. M. In Primary Processes in Photobiology; Kobayashi, T., Ed.; Springer-Verlag: Berlin, 1987, p 61.

11. Klimov, V. V.; Klevanik, A. V.; Shuvalov, V. A.; Krasnovsky, A. FEBS. Lett. 1977, 82, 183.

12. van Gorkom, H. J. Photosyn. Res. 1985, 6, 97.

13. Wasielewski, M. R.; Johnson, D. G.; Seibert, M.; Govindjee Proc. Natl. Acad. Sci. USA, 1989, 86, 524.

14. Jankowiak, R. J.; Tang, D.; Small, G. J.; Seibert, M. J. Phys. Chem., 1989, 93, 1649.

15. Owens, T. G.; Webb, S. P.; Mets, L.; Alberte, R. S.; Fleming, G. R. Proc. Natl. Acad. Sci. USA 1987, 84, 1532.

16. Wasielewski, M. R.; Fenton, J. M.; Govindjee Photosyn. Res. 1987, 17, 181.

17. Golbeck, J. H. J. Membrane Sci. 1987, 33, 151.

18. Rutherford, A. W.; Heathcote, P. Photosyn. Res. 1985, 6, 295.

19. Mathis, R.; Rutherford, A. W. In Photosynthesis; Amesz, J., Ed.; Elsevier: Amsterdam, 1987, p 63.

20. Malkin, R. In The Light Reactions; Barber, J., Ed.; Elsevier: Amsterdam, 1987, p 495.

21. Malkin, R.; Ortiz, W.; Lam, E.; Bonnerjea, J. Physiol. Veg. 1985, 23, 619.

22. Ortiz, W.; Lam, E.; Ghiradi, M.; Malkin, R. Biochim. Biophys. Acta 1984, 766, 505.

23. Lam, E.; Ortiz, W.; Mayfield, S.; Malkin, R. Plant Physiol. 1984, 74, 650.

24. Haworth, P.; Watson, J. L.; Arntzen, C. J. Biochim. Biophys. Acta 1983, 724, 151.

25. Deisenhofer, J.; Epp, O.; Miki, K.; Huber, R.; Michel, H. J. Mol. Biol. 1984, 180, 385.

26. Deisenhofer, J.; Epp, O.; Miki, K.; Huber, R.; Michel, H. Nature 1985, 318, 618.

27. Michel, H.; Epp, O.; Deisenhofer, J. EMBO J. 1986, 5, 2445.

28. Michel, H.; Deisenhofer, J. Chemica Scripta 1987, 27B, 173.

29. Chang, C. -H.; Tiede, D.; Tang, J.; Smith, U.; Norris, J.; Schiffer, M. FEBS Lett. 1986, 205, 82.

30. Allen, J. P.; Feher, G.; Yeates, T. O.; Rees, D. C.; Deisenhofer, J.; Michel, H.; Huber, R. Proc. Natl. Acad. USA 1986, 83, 8589.

31. Ford, R. C.; Picot, D.; Garavito, P. M. EMBO J. 1987, 6, 1581.

32. Witt, I.; Witt, H. T.; Gerken, S.; Saenger, W.; Dekker, J. P.; Roegner, M. FEBS Lett. 1987, 221, 260.

33. Gorokhovski, A. A.; Kaarli, R. K.; Rebane, L. A. JETP Lett. 1974, 20, 216.

34. Hayes, J. M.; Small, G. J. Chem. Phys. 1978, 27, 151.

35. Small, G. J. In Spectroscopy and Excitation Dynamics of Condensed Molecular Systems; Agranovich, V. M., Hochstrasser, R. M., Eds.; North-Holland: Amsterdam, 1983, p 515.

36. Anderson, P. W.; Halperin, B. I.; Varma, C. M. Phil. Mag. 1972, 25, 1.

37. Phillips, W. A. J. Low Temp. Phys. 1972, 7, 351.

38. Jankowiak, R.; Small, G. J. Science 1987, 237, 618.

39. Persistent Spectral Hole Burning: Science and Application; Moerner, W. E., Ed.; Springer-Verlag: West Berlin, 1988.

40. Freidrich, J.; Haarer, D. Angew. Chem., Int. Ed. Engl. 1984, 23, 113.

41. Hayes, J. M.; Gillie, J. K.; Tang, D.; Small, G. J. Biochim. Biophys. Acta 1988, 932, 287.

42. Freidrich, J.; Haarer, D. In Optical Spectroscopy of Glasses; Zschokke, I., Ed.; Reidel: Dordecht, Netherlands, 1986, p 149.

43. Optical Linewidths in Glasses, J. Lumin. 1987, 4&5, 1987.

44. van den Berg, R.; Visser, A.; Völker, S. Chem. Phys. Lett. 1988, 144, 105.

45. Berg, M.; Walsh, C. A.; Narasimhan, L. R.; Littau, K. A.; Fayer, M. D. Chem. Phys. Lett. 1987, 139, 66.

46. Fearey, B. L.; Carter, T. P.; Small, G. J. Chem. Phys. 1986, 101, 279.

47. Fearey, B. L.; Small, G. J. Chem. Phys. 1986, 101, 269.

48. Mullet, J. E.; Burke, J. J.; Arntzen, C. J. Plant Physiol. 1980, 65, 814.

49. Golbeck, J. H. Methods in Enzymol. 1980, 69, 129.

50. Carter, T. P. Ph. D. Dissertation, Iowa State University, 1986.

51. Fearey, B. L.; Carter, T. P.; Small, G. J. J. Phys. Chem. 1983, 87, 3590.

SECTION I.

PHOTOCHEMICAL HOLE BURNING OF P700

SECTION I. PHOTOCHEMICAL HOLE BURNING OF P700

INTRODUCTION

The determination of the structure of the reaction center (RC) of Rhodopseudomonas viridis [1-4] and subsequently Rhodobacter sphaeroides [5,6] has given new impetus to the debate concerning the description of the excited electronic states of the RC pigment complex. That is, the debate has turned from a discussion of which pigments comprise the RC and their arrangement to how the pigments interact to efficiently stabilize the electron in the charge transfer process [7-10].

The structure of the RC is shown in Fig. 1. It is comprised of a special pair bacteriochlorophyll dimer [P], two accessory bacteriochlorophylls [B], two bacteriopheophytins [H], a quinone, and an nonheme iron. The RC complex possesses an approximate C_2 symmetry with the two arms labeled L and M for light weight and medium weight protein structures. The center to center distances between pigments are given in Å. Upon excitation of the special pair (the primary electron donor [PED]), an electron is transported down the the L branch and is stabilized at the quinone [7-9]. This is the source of the transmembrane charge separation that drives photosynthesis.

Several remarkable photophysical features present themselves. The first important feature is that the absorption band of the PED is displaced to the red ~2200 cm^{-1} for Rps. viridis from the monomer absorption in solution [10]. A similar shift is observed for Rb. sphaeroides [7]. The cause of the shift is best associated with excitonic interactions and this led to the hypothesis of the special

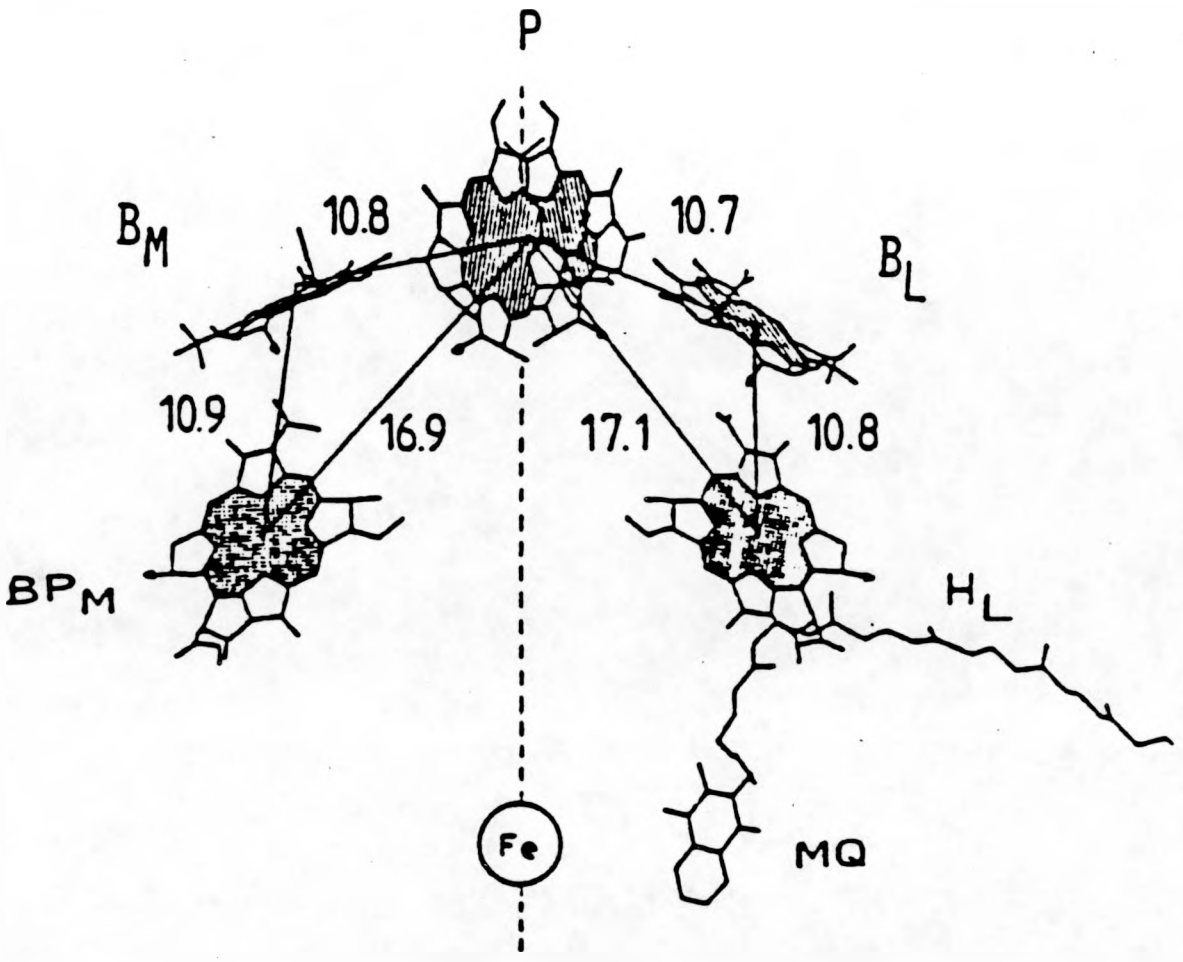

Figure 1. An overview of the structure of the reaction center of Rhodopseudomonas viridis. The center-to-center distances are given in A. P - special bacteriochlorophyll dimer; B - accessory bacteriochlorophyll; H - bacteriopheophytin; MQ - menaquinone; Fe non-heme iron.

pair [11,12]. The pigment interactions are now believed to be more complicated and current models generally mix charge transfer characteristics into the exciton manifold [13] or extend the dipole interaction to include all the RC pigments [14-16].

A second interesting feature is the observation that the e^- transfer occurs only along the L branch of the RC [7-9]. Currently, research here is focused on the role of the RC proteins. Fortuitous placement of point charges from amino residues of the surrounding protein complex can alter the relative energetic positions of electronic states [4,8,17-19]. Protein vibrations may also be important in the events leading to stabilized charge separation [20-23].

A third feature is that the transfer of the e^- from the special pair to the BPh occurs in about 3 psec [24] at room temperature apparently without the involvement of the accessory BChl molecule [7,8]. By 1986, experiments monitoring the BChl and BPh absorption with a few psec resolution had confirmed, at least on this time scale, no involvement of the accessory BChl in the e^- transport process [26, 27 and refs. therein]. It is interesting from a dynamical viewpoint how an e^- could transfer over 17Å at such rates (the rate is generally thought to depend on $\exp(-2\alpha R)$ with $\alpha \sim 0.7$ A^{-1} and R the intermolecular distance [8,28]) without accessory BChl involvement.

Several proposals have been forwarded to address the role of the accessory BChl. The most straightforward proposal is that the time scale of the special pair $\rightarrow$ BChl electron transfer is faster than the time resolution of the picosecond absorption experiments. In this case the charge separated state involving the BChl monomer is a real intermediate state in the e^- transfer. Recent experiments with 100 femtosecond time resolution did not find evidence for direct BChl participation in e^-

transfer [7,8,24,25]. A second proposal is that the e^- reaction occurs via a superexchange mechanism. In this case the state involving the BChl monomer is considered a virtual state and is not observed because it lies at an energy higher than P^* [9,29-33]. The description of the states (charge transfer character, excitonic character) and their relative energetic ordering is much debated [31,32].

Spectral hole burning is a frequency domain technique and as such circumvents the time domain problems of producing ultrafast light pulses (in the required wavelength range) and detecting ultrafast absorption changes. Using transient spectral hole burning , Boxer et al. [34,35] and Meech et al. [36,37] recorded the hole burned spectrum of the PED for Rb. sphaeroides and Rps. viridis. The holes produced were ~400 cm^{-1} broad which gives,, if the hole is homogeneously broadened, an excitation depopulation lifetime of the initial excited state of ~ 25 fsec. There are, however, two important observations. The first is that the hole maximum is not necessarily coincident with the burn frequency, and secondly the hole position remains invariant (or slightly varying) to changes in the burn wavelength. Boxer et al. [34,35] suggested that the hole may be dominated by phonon bands that result from very large displacement of the PED excited state potential surface thereby suppressing a narrow zero-phonon line. One possible mechanism for the large displacement would be direct excitation of a charge transfer state with significant charge transfer character [35,37].

Hayes and coworkers [38,39] explored the effect a highly displaced excited state would have on the observed absorption and hole profile of the PED. The spectra were modeled in terms of an arbitrarily strong electron-phonon coupling . This approach is consistent with the displacement of the excited state in a charge transfer complex. The theory is fully developed in Paper II of this section. The

absorption and hole profiles are calculated using the electron-phonon coupling strength S, the phonon frequency and phonon linewidth, the homogeneous linewidth of the zero-phonon transition, and the inhomogeneous linewidth of the profile. The zero-phonon hole (ZPH) width corresponds to the e^- transfer rate for the special pair $\rightarrow$ BPh process [40,41]. The temperature dependence of the absorption and fluorescence, and the Stokes shift (between absorption and fluorescence maximum) are used to verify the values of the parameters used to fit the profiles. It is found that the magnitude of the electron-phonon coupling combined with the inhomogeneous broadening causes the broad holes and apparent lack of sharp zero-phonon holes. That is, for large S, multiphonon transitions dominate the spectrum. The holewidths are not a manifestation of an ultrafast charge separation process. The theory presents a unified description of the absorption profile, the hole profile, and the wavelength behavior of the holes for the PED for Rps. viridis, Rb. sphaeroides, Photosystem I, and Photosystem II.

An alternate proposal to model the spectral features is suggested by Won and Friesner [42-44]. The WF theory includes a set of low frequency inter- and intramolecular vibrational modes strongly coupled into the excitonic manifold. Lattice phonons and inhomogeneous broadening are treated phenomenologically. The crucial theoretical conjecture is the resonant coupling of a charge transfer state to the vibrationally coupled excitonic state. Once the exchange coupling strength (J in WF's notation) is "turned on" the broad absorption and hole profile results from chaotic spreading of oscillator strength caused by a breakdown of the Born-Oppenheimer approximation. Coupling to the CT state suppresses the zero-phonon line. In this picture the PED profiles are homogeneously broadened. By setting the energy gap between the special pair excited state and the CT state to Δ=2000 cm^{-1}

(the internal CT state of the special pair is higher in energy than the excited state) and the coupling strength to J=240 cm^{-1}, WF successfully models the hole burning data of Boxer and coworkers [34,35] and Meech and coworkers [36,37].

Both theories (Hayes and coworkers and WF) share certain features, e.g., inhomogeneous broadening and linear-electron vibration coupling. However, weak electron-mode coupling (i.e., S < 1) is assumed in the WF model for all modes (low frequency monomer intramolecular and phonons). The ultra-fast chaotic electronic decay due to strong coupling with some type of close lying charge-transfer is eliminates sharp features in the hole spectra for the WF model. The ZPHs include the one coincident with ω_B and the vibronic satellite holes [45]. Based on the recently obtained data for the antenna Chl a and Chl b of PSI [46,47], however, one would not expect to observe sharp vibronic satellite holes of any significant intensity since the intramolecular vibronic Franck-Condon factors are very small ($\lesssim$ 0.04) and no excited state vibrations with a frequency less than 260 cm^{-1} are active. The Franck-Condon factors for the low frequency intramolecular vibronic modes ($\lesssim$ 200 cm^{-1}) of BChl a in a glass at 5 K are estimated at $\lesssim$0.02 based on fluorescence excitation spectra [48].

A critical test of the linear electron-phonon coupling theory is the observation of a narrow zero-phonon hole coincident with the laser frequency. Both models for calculating the hole profiles for PEDs allow for such an observation. However, the conditions for this observation (J=0 and/or Δ> 2000 cm^{-1}) in the WF model causes the absorption profile to become highly structured, contrary to observation. Maslov et al. [49] had reported a sharp hole (no broad hole) coincident with the laser frequency in the PED absorption profile of the PSI reaction center from the bacteria Chlamydomonas reinhardii. If this is taken as evidence to support the linear

electron-phonon coupling model, it suggests that the excited state is radically different for green photosynthetic systems. The dynamics of charge separation and stabilization would be different for green and purple photosynthetic systems.

Paper I of this section reports spectral hole burning studies of the PSI reaction center complex P700 obtained from spinach chloroplasts. A persistent hole burned spectrum is reported that is comprised of both a broad (350 cm^{-1}) hole and a narrow zero-phonon hole. The hole shapes are modeled using the linear electron-phonon coupling theory. Paper II outlines the linear electron-phonon theory which is shown to model the absorption profiles, hole profiles, and the temperature dependent line broadening data for the PED of purple photosynthetic bacteria and the hole profiles of PHB and NPHB experiments performed on the antenna and P700 complex of PSI. Chemical bleaching and white light bleaching of P700 followed by laser irradiation of the PED produced only narrow hole coincident with the laser frequency. Thus, the possibility exists that the narrow hole is not associated with P700 that is photoactive at liquid helium temperatures. Finally, new results of spectral hole burning on P700 are presented which show production of only a broad hole. The theory of Hayes and coworkers is used to fit the profiles.

reprints removed

ADDITIONAL RESULTS

The application of spectral hole burning to the photosynthetic reaction centers of green plant and purple bacteria has provided new information about the primary electron donor (PED) states. For example, structured transient hole burned spectra exhibiting four holes are obtained for the PED state P960 [40,41] and P870 [50] of Rps. viridis and Rb. sphaeroides, respectively. The hole spectrum for P960 and P870 is comprised of several relatively broad holes including a vibronic hole of ~130 cm^{-1} that builds on the lowest energy hole denoted as X. Hole X and its associated ZPH (coincident with λ_B) can be confidently assigned to the origin transition of the PED state of Rps. viridis and Rb. sphaeroides. The widths of the ZPH yield decay times that correlate well with those determined for $P870^*$ and $P960^*$ at 10 K by ultra-fast spectroscopy [24,51]. Observation of a zero-phonon hole supports the theory of Hayes and coworkers [38,39] since the theory of Won and Friesner [42-44] does not allow such observation.

The hole spectra for P680 [52], the primary electron donor of PSII, is also structured and consist of a zero-phonon hole (5 cm^{-1} width) and a broad (~130 cm^{-1} width) hole. It bears resemblance to the hole burned spectrum of $|X\rangle^*$ for P960. The zero-phonon width yields a decay time of 1.9 psec at 4.2 K, consistent with 3 psec determined using femtosecond transient absorption at room temperature [53].

A zero-phonon hole (width ~0.29 cm^{-1}) superimposed on a broad hole (~300 cm^{-1}) was reported for P700 of PSI [54]. The zero-phonon hole width corrected for instrument resolution yielded a decay time of ~90 psec and 1.6 K. This is inconsistent with the room temperature value of <10 psec [55-58] (assuming that the T-dependence for PSI is similar to that for P960 and P870), since the low

temperature decay time for P960 and P870 is known to decrease by 2X when cooled to cryogenic temperatures [51]. It has already been suggested on the basis of chemical and white light bleaching of P700 that the narrow hole is not associated with P700 that is active at liquid He temperatures [46].

This section reports new persistent photochemical hole burn profiles for P700 of PSI. The hole profiles at 1.6 K for a wide range of burn wavelengths (λ_B) are broad (FWHM ~ 310 cm^{-1}) and for the 45:1 enriched particles studied exhibit no sharp zero-phonon hole feature coincident with λ_B. The λ_B-dependent hole profiles are analyzed using the theory of Hayes and Small [38] for hole burning in the presence of arbitrarily strong linear electron-phonon coupling. A Huang-Rhys factor S in the range 4-6 and a corresponding mean phonon frequency in the range 35-40 cm^{-1} together with an inhomogeneous line broadening of ~ 100 cm^{-1} are found to provide good agreement with experiment. The zero-point level of $P700^*$ is determined to lie at ~ 710 nm at 1.6 K while the absorption maximum lies at ~ 702 nm.

The hole burning was performed using a Ar^+ pumped ring dye laser with the laser dye LD688. The laser linewidth is ~0.002 cm^{-1}. The enriched (~45:1 Chl a:P700) Photosystem I particle from spinach chloroplast is dissolved in a glycerol: water mixture to which 1 mM ascorbic acid has been added. The solvent is buffered to pH~8.3. A computer controlled double beam spectrometer operating at resolution of ~0.2 cm^{-1} was used for hole reading. The samples were held in the dark at room temperature for a few minutes before being quickly cooled (<10 minutes) to 4.2 K. All the experiments were done at 1.6 K.

At 1.6 K the 45:1 PSI particles exhibit a principal absorption maximum near 670 nm due to Chl a of the core antenna complex and a distinct but weak shoulder

located near 700 nm, which represents P700, upper curve of Fig. 1. The three lower absorbance spectra correspond to burns of 1, 5 and 10 min with I_B= 5 $\mu W/cm^2$ and λ_B = 701.8 nm. No ZPH could be observed coincident with this λ_B-value or several other values in the range between 701 and 715 nm. Under comparable burning conditions and read resolution, the earlier studied 35:1 particles exhibited a readily discernible, albeit weak, ZPH coincident with λ_B. From Fig. 2 it is apparent that the P700 hole is broad (Δ OD spectra are shown later).

The increase in absorption to higher energy of ~ 700 nm seen in the upper spectrum of Fig. 1 is due to the onset of the Chl a antenna absorption. Figure 2 shows a series of hole burned spectra obtained with λ_B= 693.2 nm (the upper spectrum is the pre-burn spectrum). At this wavelength absorption by the core antenna complex is dominant but there is some absorption due to the high energy side of the P700 absorption profile. The second and third curves of Fig. 2 are the hole burned spectra obtained with I_B = 5 $\mu W/cm^2$ for burn times of 1 and 10 min. Although not apparent from the figure, a weak ZPH is observed for the 10 min burn. The lowest spectrum of Fig. 2 was obtained after an additional 5 min burn with I_B= 2 W/cm^2 and clearly shows a ZPH coincident with λ_B. The ZPH is ascribed to NPHB of the antenna Chl a [46,47] and not P700 since the ZPH could not be observed for λ_B-values selective for P700. Although excitation transport within the core antenna complex is significantly slower at 1.6 K than at room T, the quantum efficiency for excitation trapping by P700 is still close to unity [47]. On the other hand, the NPHB quantum efficiency for the antenna Chl a is significantly less than unity [59,60]. This explains why the ZPH develops at higher burn fluences than the P700 hole.

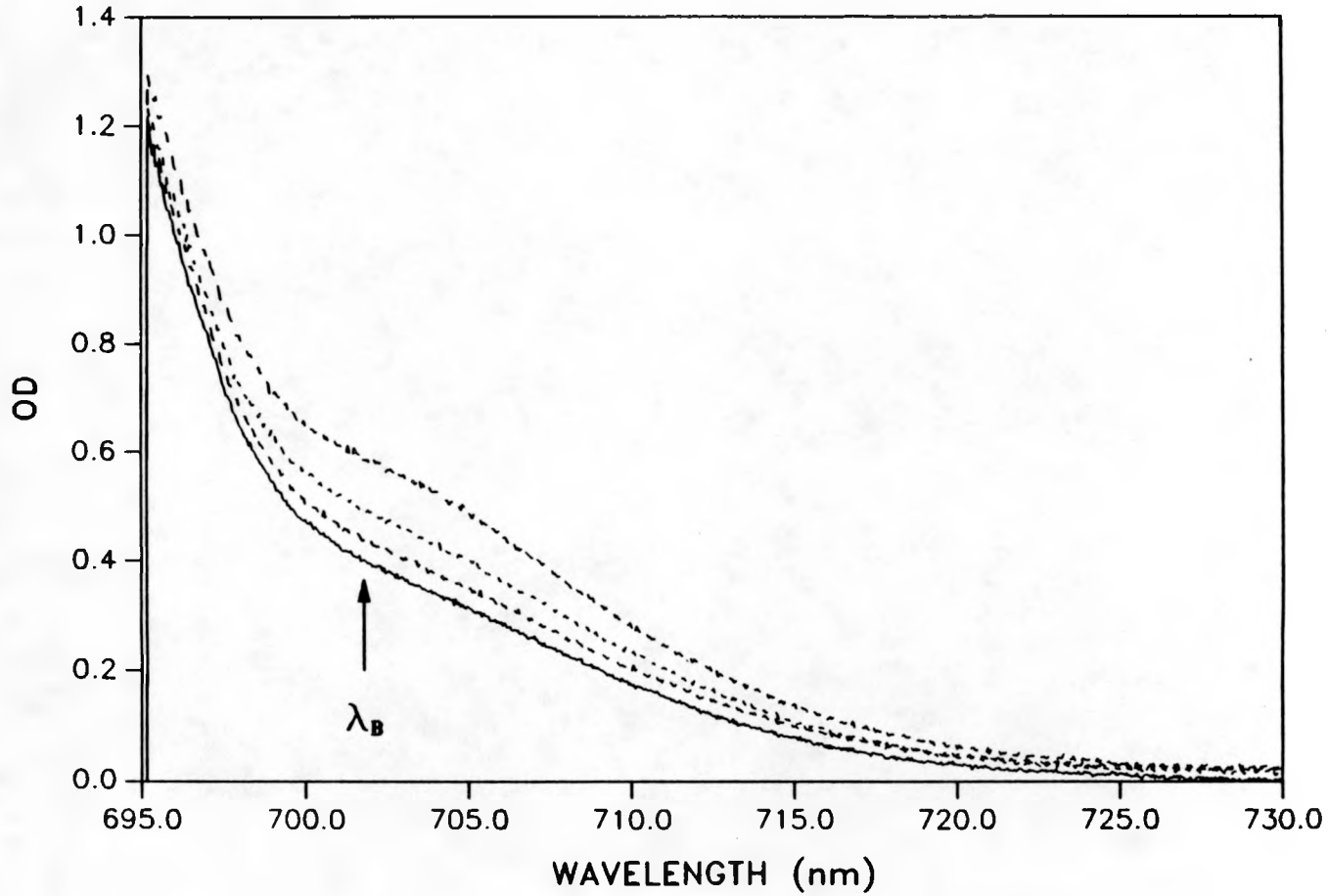

Figure 1. Burn time dependence of the P700 bleaching at 1.6 K for 45:1 PSI particles, λ_B= 701.8 nm, T = 1.6 K. The top curve is the preburn spectrum. Burn times (second to fourth) are 1, 5, 10 min with burn intensity $I_B = 5\ \mu W/cm^2$.

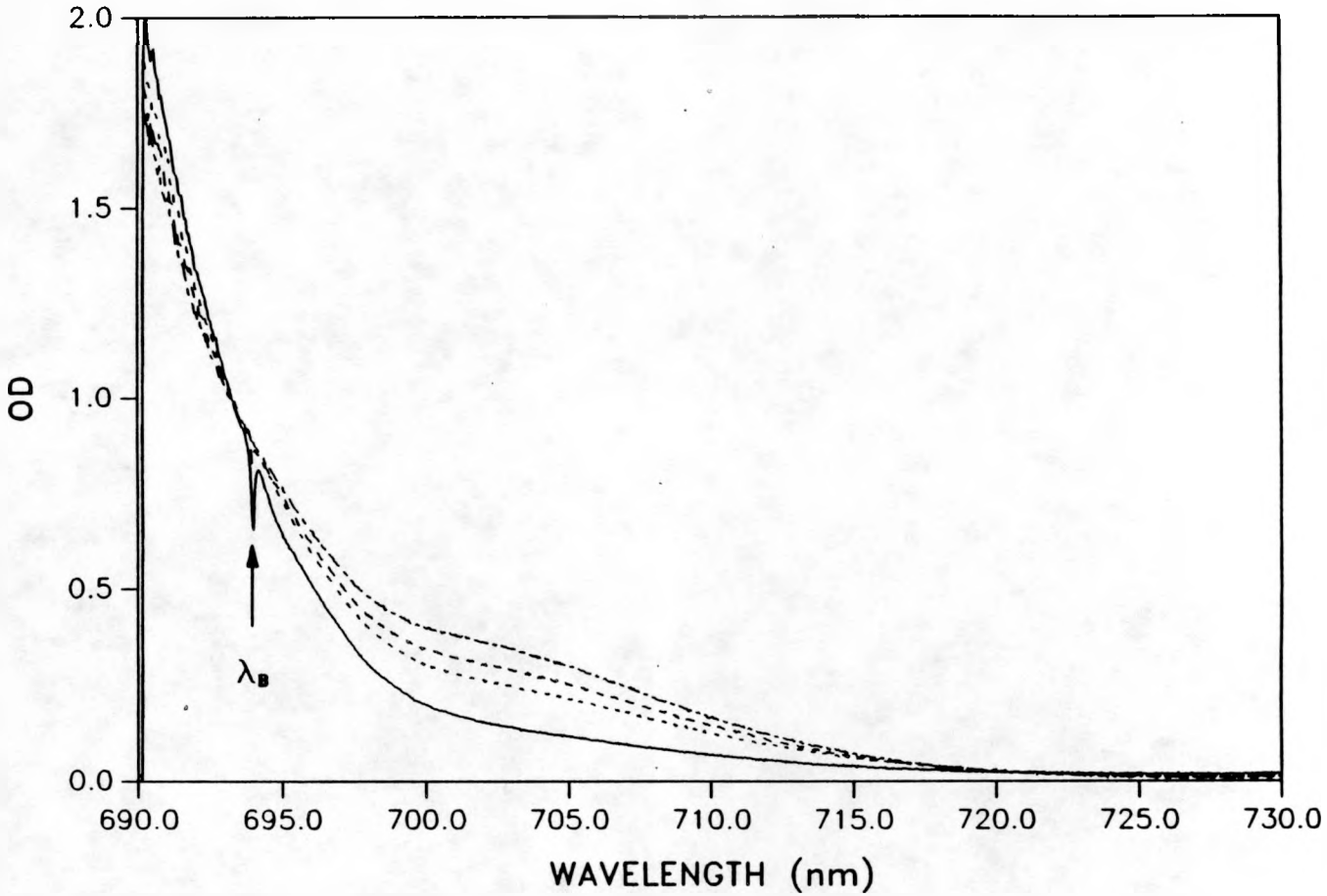

Figure 2. Burn time dependence of the P700 bleaching for 45:1 particles, λ_B = 693.2 nm, T= 1.6 K. The upper spectrum is the preburn spectrum. Burn times for the second and third spectra are 1 and 10 min, respectively, with $I_B = 5\ \mu W/cm^2$. The lowest spectrum was obtained by an additional 5 min burn with $I_B = 2\ W/cm^2$. The ZPH is ascribed to NPHB of the antenna Chl a, see text.

Figure 3 shows the ΔOD hole burned spectrum obtained with λ_B = 680.5 nm, which is close to the maximum of the antenna Chl a absorption at 670 nm. At 680.5 nm the P700 absorption is negligible. The saturated ZPH at λ_B, due to NPHB of antenna Chl a, is intense and accompanied by the real- and pseudo-PSBH (displaced by $\omega_m \sim 20\ cm^{-1}$) [46,47]. The broad positive going feature at ~ 675 nm is the anti-hole associated with NPHB [47]. The increase in noise in the vicinity of the anti-hole is due to the high O.D. near the absorption maximum. The broad P700 hole, produced by trapping of the antenna excitation, is also evident in the figure with a maximum near 702 nm.

The P700 ΔOD hole profiles obtained for λ_B = 715.0 and 706.5 nm are shown in Fig. 4 and the profile for λ_B = 702.6 nm in Fig. 5. The absorption by the antenna Chl a at these wavelengths is weak in comparison to P700. The maxima of the P700 holes for λ_B = 715.0, 706.5 and 702.6 nm are located at 705, 703 and 702 nm, respectively, and again, no sharp ZPH is observed coincident with λ_B. The solid curves are fits to the spectra obtained using the theory of Hayes and Small [38] (see also Paper II of this section).

Application of the theory to the hole profiles of P700 is more difficult than for the other PED states, e.g., P680, since resolved phonon structure and the ZPH are not observed. Futhermore, the Stokes shift associated with the P700 emission (~ $2S\omega_m$) is not known. However, we can determine that $S \gtrsim 4.5$. Otherwise, a ZPH coincident with ω_B should have been observed (given the signal/noise ratio of our spectra) for $\gamma = 1\ cm^{-1}$. This value of γ corresponds to the lifetime of P700 determined at ice temperature [58]. If this lifetime were to decrease by a factor of about 2 in the low temperature limit, which is a possibility given the data for P870 [24,51], P960 [51] and P680 [52,53], a value of S closer to 4 would preclude

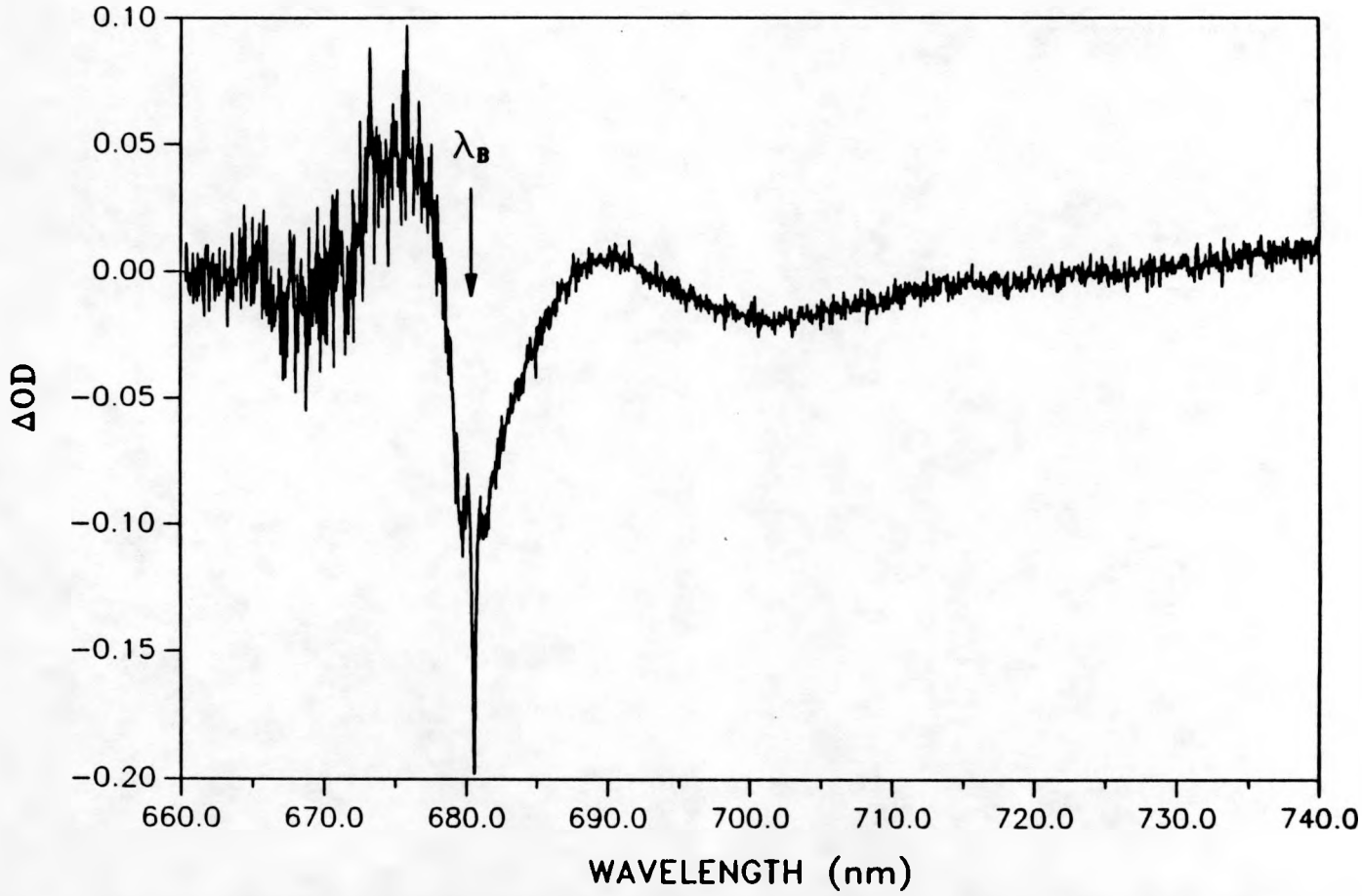

Figure 3. Difference absorbance (ΔOD) hole burned spectrum of P700 for 45:1 particles, λ_B= 680.5 nm, T = 1.6 K. Excitation was for 10 min with I_B = 50 μW/cm^2. The ZPH at λ_B and phonon sideband holes displaced from λ_B by ~ 20 cm^{-1} are due to NPHB, see text. The broad hole centered at ~ 702 nm is due to bleaching of the P700 absorption profile. For the spectrum shown here, saturation of the ZPH and phonon sideband holes gives the false impression that the linear electron-phonon coupling is stronger than reported earlier for antenna Chl a[see Section II]. The increase in noise int the anti-hole region near 675 nm is due to the high O.D. of the sample near the absorption maximum (~ 670 nm).

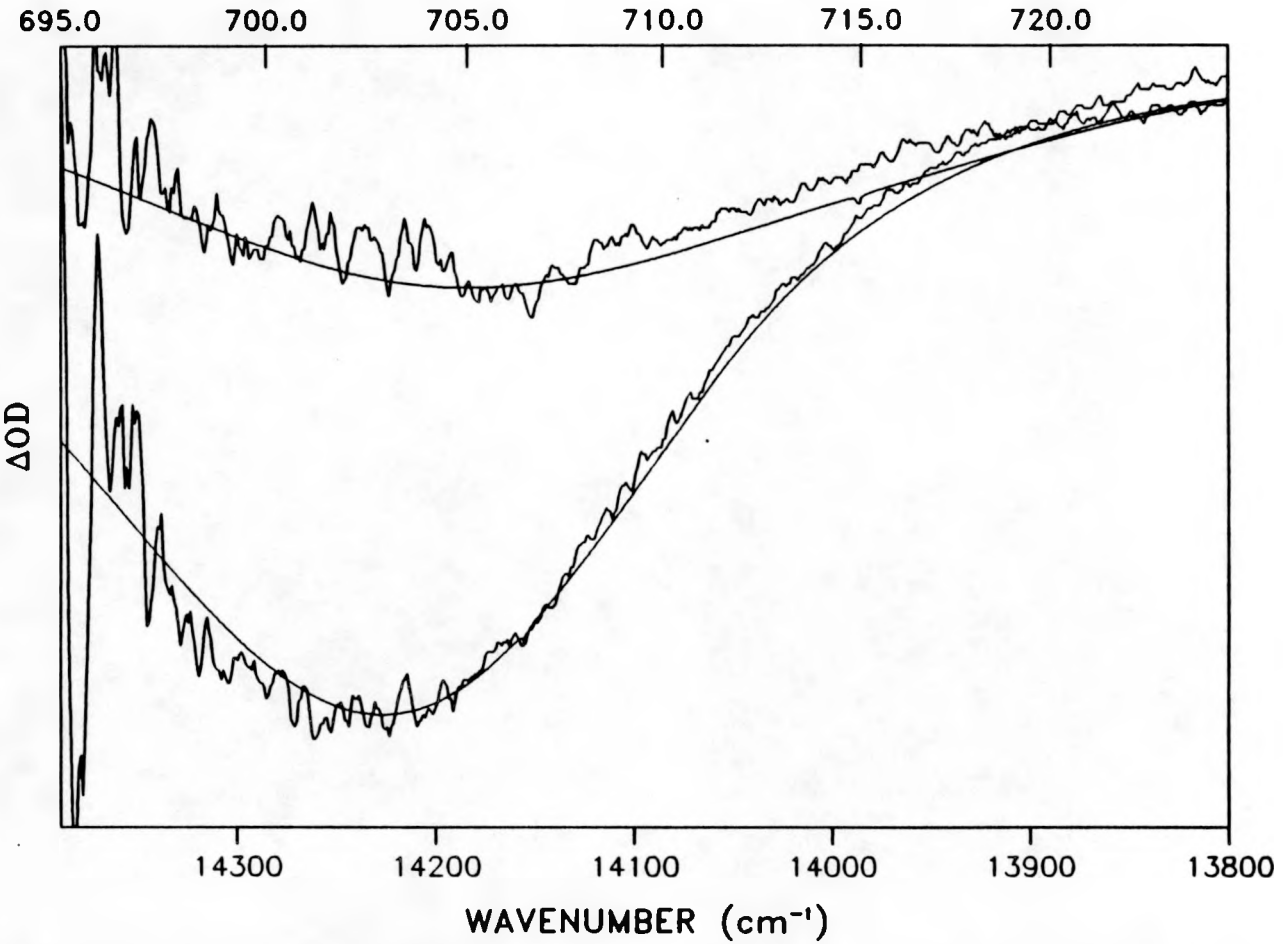

Figure 4. Difference absorbance hole burned spectra of P700 for 45:1 particles, λ_B= 715.0 nm and = 706.2 nm (top to bottom, respectively), T = 1.6 K. The ΔOD scale is 0.2. Burn time was 30 sec with I_B= 10 $\mu W/cm^2$. The solid lines are computed fits with S = 4.5, ω_m= 45 cm^{-1}, Γ_I= 1 cm^{-1}, γ= 1 cm^{-1}, and ν_m = 14085 cm^{-1}. The calculated spectrum for λ_B = 715 nm exhibits a very weak ZPH which could not be expected to be observable given the signal to noise ratio of the experimental spectrum. The top ordinate scale is wavelength (nm).

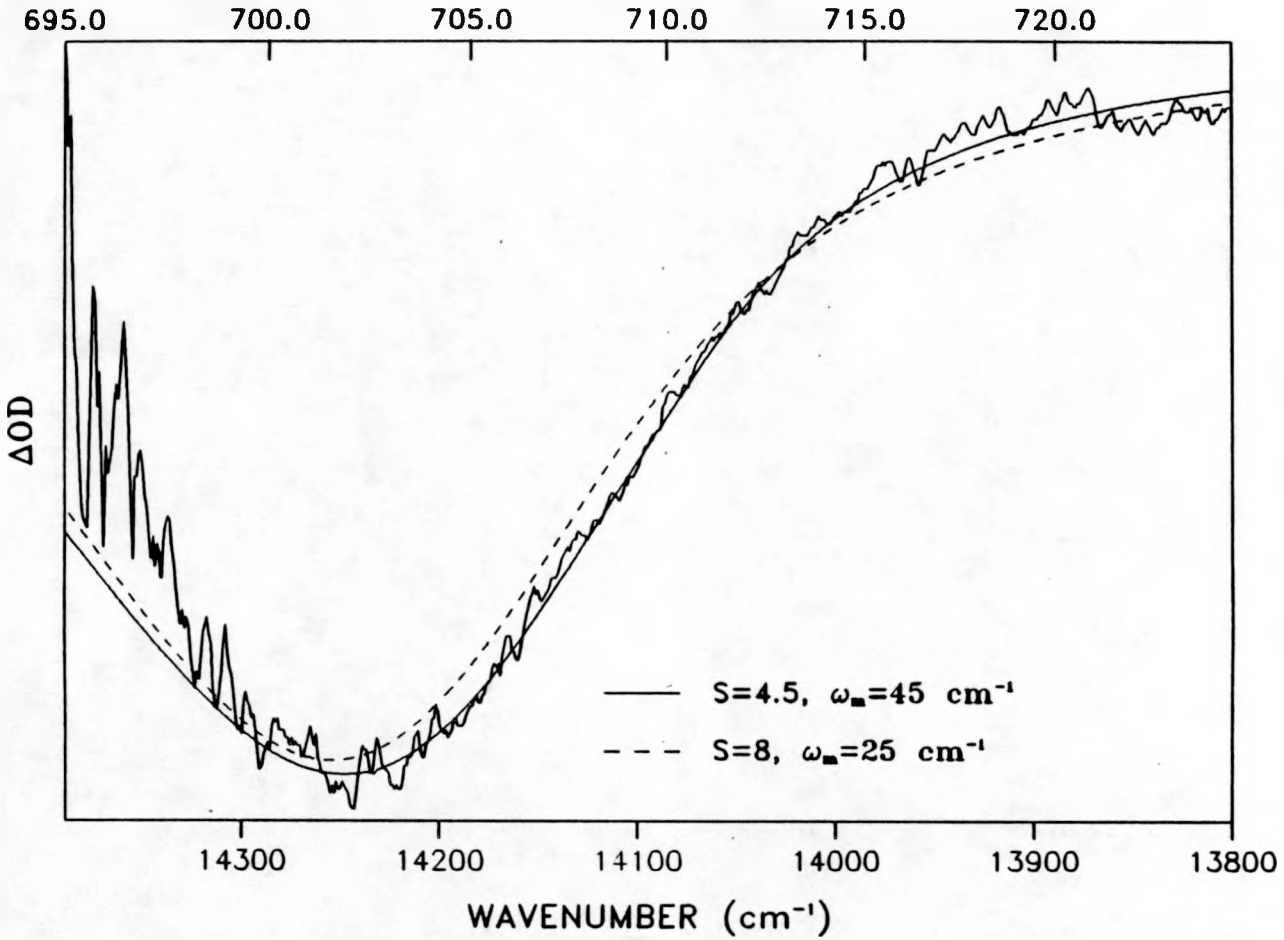

Figure 5. Difference absorbance hole burned spectrum of P700 for 45:1 particles, λ_B= 702.6 nm, T = 1.6 K. The ΔOD scale is 0.2. Burn time was 30 sec with I_B= 10 μW/cm^2. The solid and broken lines are computed fits with S = 4.5 and ω_m = 45 cm^{-1} (—) or S = 8 and ω_m = 25 cm^{-1} (---). See Fig. 5 caption for other parameter values. The top ordinate scale is wavelength (nm).

observation of the ZPH in our spectra for PSI-45. In our earlier work with PSI-35 particles [54] a value of S = 5.5 was used to fit the hole spectra of P700 because the observed ZPH with a width of only ~ 0.05 cm^{-1} was assumed to be due to P700. The present and other [39,46] studies indicate that it is not, vide infra.

The modest λ_B-dependence of the P700 hole profile maxima shown here, as well as that measured from λ_B = 708.2, 701.8 and 693.2 nm spectra, indicate that $\Gamma_I < S\omega_m$. The hole maxima for these three λ_B values are located at 703, 702 and 701 nm, respectively. One is constrained in the choice of the center (ν_m) of the zero-phonon transition frequency by the observed λ_B-dependence [38,39] and the requirement that the calculated absorption spectrum must provide agreement with the observed spectrum. The calculated hole profiles in Figs. 4 and 5 for S = 4.5, ω_m = 45 cm^{-1}, Γ_I = 100 cm^{-1}, Γ = 60 cm^{-1} and ν_m = 14085 cm^{-1} (710 nm) provide reasonable agreement with the observed profiles. The deviations on the high energy side of the hole maxima are the result of the appearance of an increase in absorption (with a maximum near 690 nm [54,61,62]) which has been attributed to an electrochromic shift of the Chl a in the near proximity of the RC [61,62]. Thus, the quality of fit of the theoretical profiles can only be judged on the basis of the region of the experimental profiles in the vicinity of the hole maximum and to lower energy of the maximum. The P700 absorption spectrum calculated with the above parameter values is shown in Fig. 6. The calculated profile exhibits a maximum at 701.5 nm and a width of 350 cm^{-1}. From the theory one expects [39] that the calculated absorption width should be given roughly by $S\omega_m + \Gamma_I$ (300 cm^{-1} in this case).

Chemical and white light bleaching experiments on PSI-35 particles discussed by Gillie and coworkers [46] and Hayes and coworkers [39] had indicated that the

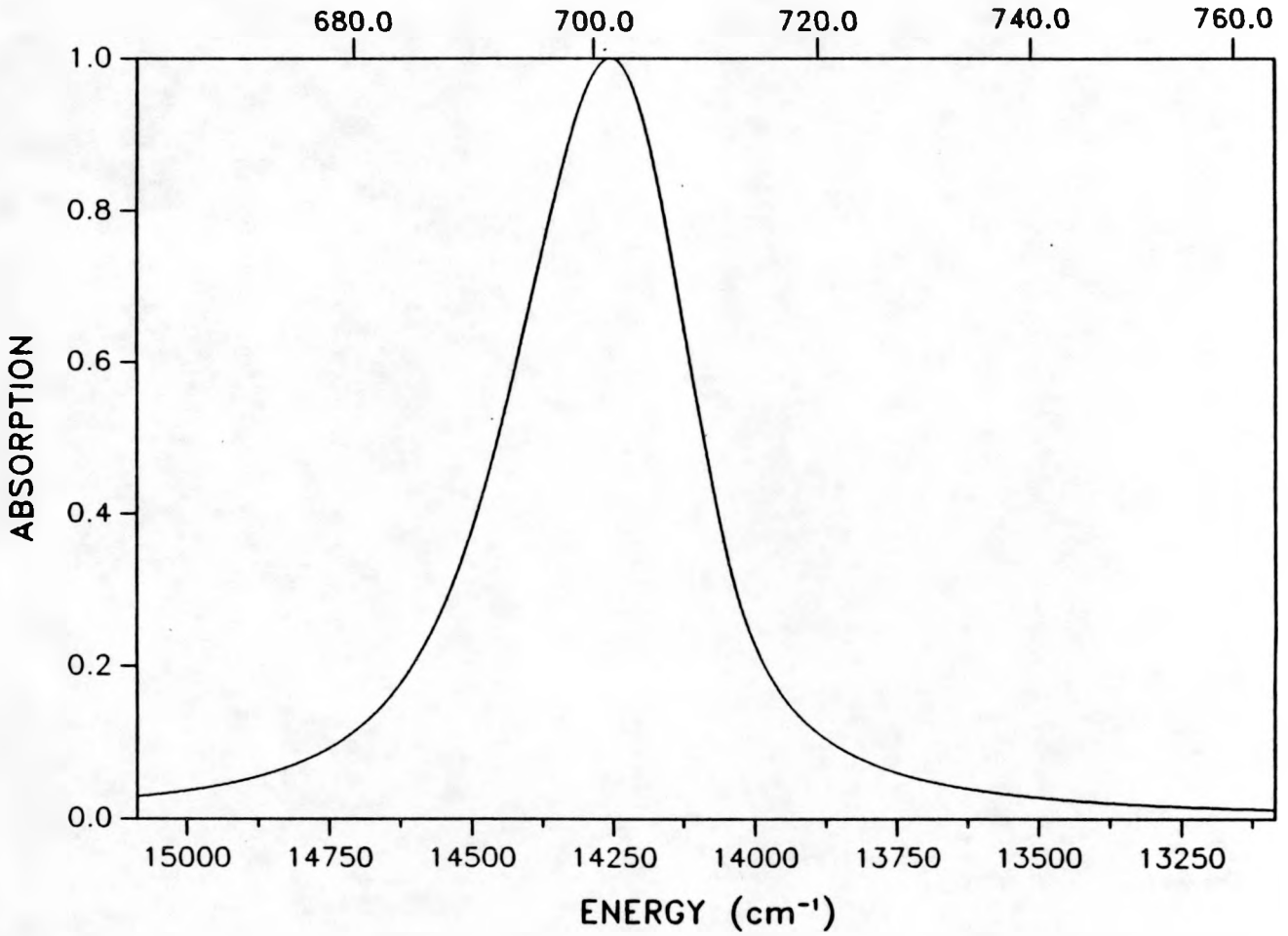

Figure 6. Calculated absorption profile for P700 at 1.6 K. The parameters used were S = 4.5, ω_m= 45 cm^{-1}, Γ_I= 100 cm^{-1}, γ= 60 cm^{-1}, γ= 1 cm^{-1}, and ν_m = 14085 cm^{-1} (710 nm).

sharp ZPH reported earlier [54] for P700 of PSI-35 particles is not due to photoactive P700. The present results for PSI-45 particles confirm this. With the enrichment procedure described by Golbeck [63] we have found that an enrichment of ~ 35:1 is more difficult to attain than an enrichment of ~ 45:1. This suggests, perhaps, that the 35:1 particles could be subject to a higher probability for damage than the 45:1 particles. The sharp but weak ZPH reported for the 35:1 particles could be due to inactive P700 or antenna Chl a perturbed by the isolation procedure. In any event, a hole width of 0.05 cm^{-1} [46] translates to a minimum depopulation decay time for P700 at 1.6 K of 210 psec, which is difficult to reconcile in view of the measured decay times at room T [58,64,65] and the fact that the decay rates for $P870^*$ [24,51], P960 [51] and $P680^*$ [52,53] increase as the temperature is decreased from room T.

Turning now to the application of the theory to the ΔOD spectra shown in Figs. 4 and 5 it can be seen that the parameter values S= 4.5, ω_m= 45 cm^{-1}, Γ = 60 cm^{-1}, Γ_I = 100 cm^{-1} and ν_m = 14085 cm^{-1} provide reasonable fits to the observed profiles. In fitting to the spectra, Γ was held constant at 60 cm^{-1}, a value that is about twice that observed for the antenna Chl a [47]. The increase in Γ was scaled according to the ratio of the ω_m value utilized for P700 to that observed for the antenna Chl a. We hasten to add that the comparable theoretical fits to the P700 hole profiles could be achieved using two or more mean phonon frequencies. However "multi-phonon" fits are not justified at this time since the underlying structure for P700 has not been observed. It was found that the λ_B-dependence of the hole maximum could not be accounted for if ν_m (λ = 710 nm) was varied by more than ±2 nm from 710 nm. The fitting of the λ_B-dependence also depends quite sensitively on the ratio $S\omega_m/\Gamma_I$ as one would expect since in the limit $S\omega_m >>$

Γ_I there should be no λ_B-dependence [39]. Comparable fits to the hole spectra can be obtained by increasing Γ_I somewhat (e.g, to 120 cm^{-1} as determined for P680 [52]) provided $S\omega_m$ is appropriately increased. This is also true if S is increased and ω_m decreased proportionately (for a fixed Γ_I). However, it was found that the goodness of fit to the low energy side of the hole profiles worsens if S is increased too much above 4.5, e.g., to 8 (Fig. 5). Our many calculations (only a few of which are shown here) indicate that S and ω_m values in the ranges 4-6 and 50-35 cm^{-1} and $\Gamma_I \sim 100$ cm^{-1} can adequately account for the observed hole profiles. The calculated absorption spectrum in Fig. 6 is difficult to compare with experiment because of the interference by the low energy tail of the antenna Chl a, see upper curve of Fig. 1. However, since the linear electron-phonon coupling is strong (i.e., the homogeneous contribution to the P700 absorption is large) the photochemical hole burning can produce a bleach that essentially encompasses the entire absorption profile. In particular, for λ_B significantly to the blue of 710 nm (center of the zero-phonon excitation frequency distribution), e.g., 702.6 nm as in Fig. 5, or located in the antenna Chl a absorption origin (Fig. 3) the hole should be a faithful representation of the P700 absorption profile at 1.6 K. The calculated absorption spectrum is in good agreement with the two hole burned spectra just mentioned. Thus, we conclude that P700 exhibits a maximum at ~ 702 nm and a FWHM of 350 cm^{-1} at 1.6 K. Approximately 30 and 70% of this width is due to inhomogeneous broadening (from linear electron-phonon coupling), respectively.

From the results presented here for P700 it is apparent that the P700 hole spectra are significantly different from those for the other PED states P680, P870 and P960. Although here appear to be significant differences [20,66] between the interactions of the special pair and amino acid residues in Rps. viridis and Rb.

sphaeroides the similarity in their cofactor structures [67] is sufficient to yield very similar hole spectra for P960 and P870. The hole spectra for P700 show no evidence of any structure (akin to that associated with the ~ 130 cm^{-1} mode of P870 and P960) even though the P700 hole profile and calculated absorption profile are about 100 cm^{-1} narrower than the overall hole widths and absorption widths of P870 and P960. This, together with the fact that Γ_I ~ 100 cm^{-1} for P700, is telling in the sense that if a mode analogous to the 130 cm^{-1} is active in the P700 hole profile, the fact that it cannot be resolved means that its frequency is considerably reduced. We cannot distinguished between this possibility or the possibility that such a progression forming mode does not exist. The existence of the special pair for P700 is still being debated but evidence for its existence appears to be mounting. Assuming that it does exist, the above remarks and the absence of the ZPH for P700 indicate that its geometric and electronic structure of its excited state may be quite different from those for the purple bacteria. The absence of the ZPH for P700 indicates that $S \gtrsim 4.5$ and, therefore, that the coupling of $P700^*$ with low frequency phonons is stronger than for $P870^*$, $P960^*$ and $P680^*$ whose S-values are close to 2. The strong linear electron-phonon coupling for $P700^*$ suggests that it may possess significant charge-transfer character as is the case for $P870^*$ [69-71] and $P960^*$ [69,71,72].

CONCLUSIONS

Spectral hole burning studies performed by this group have demonstrated that the hole burning characteristics for the PED states P960, P870, P680, and P700 are similar and defined by strong electron-phonon coupling and significant site inhomogeneous broadening. The exact description of the PED states, neutral exciton with significant intra-dimer charge transfer character or admixtures of P^* and a charge transfer between P and other reaction center pigments, is left unresolved. A dimer structure for P700 is indicated.

REFERENCES

1. Deisenhofer, J.; Epp, O.; Miki, K.; Huber, H. J. Mol. Biol. 1984, 180, 385.

2. Deisenhofer, J.; Epp, O.; Miki, K.; Huber, R.; Michel, H. Nature 1985, 318, 618.

3. Michel, H.; Epp, O.; Deisenhofer, J. EMBO J. 1986, 5, 2445.

4. Michel, H.; Deisenhofer, J. Chemica Scripta 1987, 27B, 173.

5. Allen, J. R.; Feher, G.; Yeates, T. O.; Rees, D.C.; Deisenhofer, J.; Michel, H.; Huber, R. Proc. Natl. Acad. Sci. USA 1986, 83, 8589.

6. Chang, C. H.; Teide, D.; Tang, J.; Smith, U.; Norris, J.; Schiffer, M. FEBS Lett. 1986, 205, 82.

7. Kirmaier, C.; Holten, D. Photosynth. Res. 1987, 13, 225.

8. Budil, D. E.; Gast, P.; Chang, C. H.; Schiffer, M.; Norris, J. Ann. Rev. Phys. Chem. 1987, 38, 561.

9. Michel-Beyerle, M. E.; Plato, M.; Deisenhofer, J.; Michel, H.; Bixon, M.; Jortner, J. Biochim. Biophys. Acta 1988, 932, 52.

10. Parson, W. W.; Scherz, A.; Warshel, A. In Antennaand Reaction Centers of Photosynthetic Bacteria: Michel-Beyerle, M. E., Ed.; Springer-Verlag: Berlin, 1985, p 122.

11. McElroy, J. D.; Mauzerall, D. C.; Feher, G. Biochim. Biophys. Acta 1972, 267, 363.

12. Norris, J. R.; Uphaus, R. A.; Crespi, H. L.; Katz, J. J. Proc. Natl. Acad. Sci. USA 1971, 68, 625.

13. Warshel, A.; Parson, W. W. J. Amer. Chem. Soc. 1987, 109, 6143; J. Amer. Chem. Soc. 1987, 109, 6152.

14. Zinth, W.; Knapp, E. W.; Fischer, S. F.; Kaiser, W.; Deisenhofer, J.; Michel, H. Chem. Phys. Lett. 1985, 119, 1.

15. Knapp, E. W.; Scherer, P. O. J.; Fischer, S. F. Biochim. Biophys. Acta 1986, 852, 295.

16. Scherer, P. O. J.; Fischer, S. F. Biochim. Biophys. Acta 1987, 891, 157.

17. Rackovsky, S.; Scher, H. Biochim. Biophys. Acta 1982, 681, 152.

18. Scherer, P. O. J.; Fischer, S. F. Chem. Phys. Lett. 1987, 141, 179.

19. Warshel, A.; Creighton, S.; Parson, W. W. J. Phys. Chem. 1988, 92, 2696.

20. Yeates, T. O.; Komiya, H.; Chirino, A.; Rees, D. D.; Allen, J. P.; Feher, G. Proc. Natl. Acad. Sci. USA 1988, 85, 7993.

21. Teide, D. M.; Kellog, E.; Breton, J. Biochim. Biophys. Acta 1987, 892, 294.

22. Creighton, S.; Hwang, J. K.; Warshel, A.; Parson, W. W.; Norris, J. Biochemistry 1988, 27, 774.

23. Robert, B.; Lutz, M. Biochemistry 1988, 27, 5108.

24. Martin, J. L.; Breton, J.; Hoff, A. J.; Migus, A.; Antonetti, A. Proc. Natl. Acad. USA 1986, 83, 957.

25. Breton, J.; Martin, J. L.; Migus, A.; Antonetti, A.; Orszag, A. Proc. Natl. Acad. Sci. USA 1986, 83, 5121.

26. Holten, D.; Hoganson, C.; Windsor, M. W.; Schenck, C. C.; Parson, W. W.; Migus, A.; Fork, R. L.; Shank, C. V. Biochim. Biophys. Acta 1980, 952, 461.

27. Kirmaier, C.; Holten, D.; Parson, W. W. FEBS Lett. 1985, 185, 76.

28. Hopfield, J. J. Proc. Natl. Acad. Sci. USA 1974, 71, 3640.

29. Marcus, R. A. Chem. Phys. Lett. 1987, 133, 471.

30. Bixon, M.; Jortner, J.; Michel-Beyerle, M. E.; Ogrodnik, A.; Lersch, W. Chem. Phys. Lett. 1987, 140, 626.

31. Plato, M.; Möbius, K.; Michel-Beyerle, M. E.; Bixon, M.; Jortner, J. J. Amer. Chem. Soc. 1988, 110, 7279.

32. Marcus, R. A. Chem. Phys. Lett. 1988, 133, 471.

33. Won, Y.; Freisner, R. A. Biochim. Biophys. Acta 1988, 935, 9.

34. Boxer, S. G.; Lockhart, D. J.; Middendorf, T. R. Chem. Phys. Lett. 1985, 121, 476.

35. Boxer, S. G.; Middendorf, T. R.; Lockhart, D. J. FEBS Lett. 1986, 200, 237.

36. Meech, S. R.; Hoff, A. J.; Weirsma, D. A. Chem. Phys. Lett. 1985, 121, 287.

37. Meech, S. R.; Hoff, A. J.; Weirsma, D. A. Proc. Natl. Acad. Sci. USA 1986, 83, 9464.

38. Hayes, J. M.; Small, G. J. J. Phys. Chem. 1986, 90, 4928.

39. Hayes, J. M.; Gillie, J. K.; Tang, D.; Small, G. J. Biochim. Biophys. Acta 1988, 932, 287.

40. Tang, D.; Jankowiak, R.; Gillie, J. K.; Small, G. J.; Tiede, D. M. J. Phys. Chem. 1988, 92, 4012

41. Tang, D.; Jankowiak, R.; Small, G. J.; Tiede, D. M. Chem. Phys. 1989, 131, 99.

42. Won, Y.; Friesner, R. A. Proc. Natl. Acad. Sci. USA 1987, 84, 5511.

43. Won, Y.; Friesner, R. A. In Structure of Bacterial Reaction Centers: X-ray Crystallography and Optical Spectroscopy with Polarized Light; Breton, J., Verméglio, A., Eds.; Plenum: New York, 1988, p 341.

44. Won, Y.; Freisner, R. A. J. Phys. Chem. 1988, 92, 2208; J. Phys. Chem. 1988, 92, 2214.

45. Small, G. J. In Spectroscopy and Excitation Dynamics of Condensed Molecular Systems; Agranovich, V. M., Hochstrasser, R. M., Eds.; North-Holland: Amsterdam, 1983, p 515.

46. Gillie, J. K.; Hayes, J. M.; Small, G. J.; Golbeck, J. H. J. Chem. Phys. 1987, 91, 5524.

47. Gillie, J. K.; Small, G. J.; Golbeck, J. H. J. Phys. Chem. 1989, 93, 1620.

48. Renge, I.; Mauring, K.; Avarmaa, R. J. Lumin. 1987, 37, 207.

49. Maslov, V. G.; Chunaev, A. S.; Tugarinov, V. V. Mol. Biol. 1981, 15, 788.

50. Tang, D.; Johnson, S. G.; Jankowiak, R.; Hayes, J. M.; Small, G. J.; Tiede, D. M. J. Phys. Chem., submitted.

51. Breton, J.; Martin, J. -L.; Fleming, G. R.; Lambry, J. -C. Biochemistry 1988, 27, 8276.

52. Jankowiak, R.; Tang, D.; Small, G. J.; Seibert, M. J. Phys. Chem. 1989, 93, 1649.55.

53. Wasielewski, M. R.; Johnson, D. G.; Seibert, M.; Govindjee Proc. Natl. Acad. Sci. USA 1989, 86, 524.

54. Gillie, J. K.; Fearey, B. L.; Hayes, J. M.; Small, G. J.; Golbeck, J. H. Chem. Phys. Lett. 1987, 134, 316.

55. Shuvalov, V. A.; Klevanik, A. V.; Kryulov, A. V.; Ke, B. FEBS Lett. 1979, 107, 313.

56. Shuvalov, V. A.; Ke, B.; Dolan, E. FEBS Lett. 1979, 100, 5.

57. Shuvalov, V. A.; Nuijis, A. M.; van Gorkum, H. J.; Smit, H. W. J.; Duysens, L. N. M. Biochim. Biophys. Acta 1986, 850, 319.

58. Owens, T. G.; Webb, S. P.; Mets, L.; Alberte, R. S.; Fleming, G. R. Proc. Natl. Acad. Sci. USA 1987, 84, 1532.

59. Jankowiak, R.; Small, G. J. Science 1987, 237, 618.

60. Jankowiak, R.; Shu, L.; Kenney, M. J.; Small, G. J. J. Lumin. 1987, 36, 293.

61. Schaffernicht, H.; Junge, W. Photochem. Photobiol. 1981, 34, 223.

62. Sétif, P.; Mathis, P.; Vänngård, T. Biochim. Biophys. Acta 1984, 767, 404.

63. Golbeck, J. H. In Methods in Enzymology: San Pietro, A., Ed.; Academic: New York, 1980, p 129.

64. Fenton, J. M.; Pellin, M. J.; Govindjee; Kaufmann K. J. FEBS Lett. 1979, 100, 1.

65. Wasielewski, M. R.; Fenton, J. M.; Govindjee Photosyn. Res. 1987, 12, 181.

66. Allen, J. P.; Feher, G.; Yeates, T. O.; Komiya, H.; Rees, D. C. Proc. Natl. Acad. Sci. USA 1988, 85, 8487.

67. Allen, J. P.; Feher, G.; Yeates, T. O.; Komiya, H.; Rees, D. C. Proc. Natl. Acad. Sci. USA 1987, 84, 5730; Proc. Natl. Acad. Sci. USA 1987, 84, 6162.

68. Golbeck, J. H. Biochim. Biophys. Acta 1987, 895, 167.

69. Braun, H. P.; Michel-Beyerle, M. E.; Breton, J.; Buchanan, S.; Michel, H. FEBS Lett. 1987, 221, 221.

70. Lockhart, D. J.; Boxer, S. G. Biochemistry 1987, 26, 664.

71. Lockhart, D. J.; Boxer, S. G. Proc. Natl. Acad. Sci. USA 1988, 85, 107.

72. Lösche, M.; Feher, G.; Okamura, M. Y. Proc. Natl. Acad. Sci. USA 1987, 84, 7537.

SECTION II.

NONPHOTOCHEMICAL HOLE BURNING OF THE ANTENNA COMPLEXES OF PHOTOSYSTEM I

SECTION II: NONPHOTOCHEMICAL HOLE BURNING OF THE ANTENNA COMPLEXES OF PHOTOSYSTEM I

INTRODUCTION

The majority of the chlorophyll in the photosynthetic thylakoid membrane act to collect, harvest, solar energy and transport that energy to the reaction center. Because of its overlap with the solar irradiance spectrum, limited at high energy by O_2 absorption and at low energy by H_2O overtone absorption, the first excited state Q_y transition of chlorophyll plays an important role in efficient solar energy collection. How energy deposited in the Q_y transition is transferred from spatially distant Chl to the reaction center has been extensively studied using fluorescence [1-11], picosecond absorption recovery [12-15], singlet-singlet annihilation [16-20], and spectral hole burning [21-25]. This subject has been extensively reviewed [26-31].

This section will discuss the dynamics of excitation energy transport (EET) in the light harvesting chlorophyll protein complex (LHCPI) associated with Photosystem I. In particular, results from nonphotochemical hole burning (NPHB) on the core antenna complex and LHCPI are presented to explore these questions: How are the pigments arranged in their protein environment? Is the excitation localized or delocalized within LHCPI? What roles do intramolecular vibrations and low frequency protein vibrations (phonons) play in mediating EET?

Discussions on the nature of EET in photosynthetic units (PSU) began in 1938 when Franck and Teller drew analogies to EET in crystals. "The coupling between particles in the crystals and the resonance caused by the identity of the crystal cells

has the consequence that excitation energy will be transferred from one cell to another" [32]. Franck and Teller outlined the work of Frenkel [33] and Peierls [34] that suggested the concept of excitation waves, called excitons, within crystals. Franck and Teller concluded, however, that "the existence of a PSU is improbable." The existence of the PSU has been demonstrated [35-38]. Robinson [39] gave a succinct review of the progress made in understanding EET and trapping in photosynthesis up to 1966.

Franck and Teller [32] assumed a one-dimensional PSU which is probably the main source of the error in their analysis [39]. This assumption leads to a transfer time of τ=0.01 psec which is too fast for efficient trapping at the RC [32]. Bay and Pearlstein [40,41] extended the theories to two dimensional arrays. In either case, the theories have assumed that the Chls in the antenna proteins are arranged in a regular lattice array and the exciton migration is believed to be diffusive, i.e., a noncoherent random walk through the lattice. The Chls interact in the conventional Förster dipole-dipole mechanism. It is important to understand the conditions by which exciton motion becomes incoherent, i.e., a random walk.

Mathematically, a delocalized exciton is described when the eigenfunctions for the excited state are written as superposition of excitations on the individual crystal cells [33,34]. The coefficients are made to vary sinusiodally as a function of the coordinate of the cell [33,34]. For one-dimensional excitons, the stationary states of the system Hamiltonian are

$$|k\rangle = N^{-1/2} \sum_{n} e^{i\underline{k}\cdot r_n} \; |n\rangle \qquad (1)$$

where N is the number of independent identical molecules. The states are characterized by the exciton wavevector $\underline{k}$ [42].

In large molecules the electronic transitions are coupled to intramolecular vibrations and lattice vibrations (phonons). If the exciton-phonon interaction (or lattice coupling energy) is comparable with or larger than the exciton bandwidth, the system is said to be a strong exciton scatterer [33,34]. If we consider propagation of an exciton wavepacket with a well-defined $\underline{k}$, the scattering processes act to change the $\underline{k}$-state directionality, hence the exciton loses memory of the initially prepared $\underline{k}$-state. For band transport, phonons scatter the exciton (labeled by the wavevector $\underline{k}$) between different $\underline{k}$-states. For hopping transport, phonons scatter the nearly localized exciton states (labeled by the site index $\underline{n}$) [43]. The exciton wavepacket is said to take a random walk.

However, if the exciton-phonon coupling is weak, no change in the $\underline{k}$-state description occurs and the exciton moves as a perfect wave through the system [43]. This is often referred to as "coherent" transport.

The coherent process only applies on the time scale in which the $\underline{k}$-states have a well defined relationship. A criterion for coherent exciton migration (CEM) relates the $\underline{k}$-state lifetime, $\tau(k_o)$, to the exciton mean free path, $l(k_o)$, and the group velocity, $V_g(t)$ by [42,44]

$$l(k_o) = \tau(k_o)\, V_g(t). \qquad (2)$$

The exciton defined by a wavevector with a mean value about k_o is coherent if $\tau(k_o)$ is greater than the intramolecular transfer time given by $\langle\tau\rangle = a/\langle V_g(t)\rangle$ with a being the lattice spacing [42]. The group velocity can be calculated from the nearest-neighbor interaction and distance. Physically, we see that the exciton remains in a particular $\underline{k}$-state (wavelike) for $\tau(k_o)$ until it is modulated sufficiently via scattering processes to alter the $\underline{k}$-state description [43]. The mean free path is

the distance traveled before the k-state description is altered. Prerequisites for CEM in organic crystals are low temperatures and high quality strain-free crystals [45]. For 1,2,4,5- tetrachlorobenzene, $l(k) = 300$ to 10^4 Å and $\tau(k) = 10^{-7}$ sec [44,46]. Determining $l(k)$ and $\tau(k)$ for photosynthetic systems is difficult. Recent NPHB experiments on the antenna system of P. aestuarii show that the exciton-phonon coupling is weak [47] which could suggest that CEM might occur in the light harvesting complexes of PSUs. Other descriptions of EET can be envisioned, i.e., polariton formation and migration [45,48] (the reader is referred to a special issue of Chemical Physics [see ref. 45] for discussions of EET in solids).

When discussing the problems of EET, one must be careful of the terminology. The coherent or noncoherent transfer limit is defined as above. If the excitation is localized, it is associated with a particular site. Excitation into a strongly excitonic system is necessarily delocalized since the exciton wavefunction is a superposition of the wavefunctions of the interacting molecules. No spatial transfer is needed within a subunit, in this case, since the prepared state involves all the molecules in the subunit.

Our understanding of EET in antenna systems has been greatly enhanced with the mathematical descriptions given by Knox [26,49-51], Paillotin [52-55], and Pearlstein [31,40,41,56]. These models describe the nature of the EET as random hops between Chls arranged in a regular lattice array. The conditions for this description were described earlier. This description of EET is preferred because the mathematics is simplified. In the Pearlstein model the excitation executes a random walk until it reaches a trap, a reaction center in this case. At this point it may undergo photochemical conversion or reenter the antenna to continue its random walk. The interaction between Chls is described by the Förster [57] dipole-dipole

interaction mechanism and falls off as $1/R^6$ where R is the distance between molecules. The Chls are weakly interacting. References [26,28,29,39,41,58] are good reviews of the details of the theories.

The random walk is said to be be "diffusion limited" if the photoconversion rate at the trap is faster than the time required for the excitation to reach the trap for the first time (first passage time). If the photoconversion is slower then the kinetics are "trap limited" [41].

Pearlstein [41] proposed a means of experimentally determining the first passage time. The mean lifetime of the excitation, M_o, is given by

$$M_o = [1+(F_D/F_T)(N-1)]k_p^{-1} + \{[1-p_o(0)](N-1)[(qF_T)^{-1} - (qF_A)^{-1}] + [-f_{oo} + \sum_i f_{oi}p_i(0)]NF_A^{-1}\} \quad (3)$$

where N is the Chl array size; F_T,F_D are the Förster rate constants for trapping and detrapping; F_A is the reversible Förster rate constant for hopping between nearest-neighboring antenna Chl; k_p is the photoconversion rate constant; p_i is the probability of finding the excitation on molecule i, with p_o the probability that it resides on the reaction center; q is the lattice coordination number; f_{ij}'s are lattice parameters that depend on N and the lattice structure.

In the case where the probability of exciting the RC and antenna is unknown, Eqn. 3 becomes

$$M_o=[1+(F_D/F_T)(N-1)]k_p^{-1} + (1/F_A)\{(F_A/F_T) + [q\alpha N^2)/(N-1)^2]-1\} * (N-1)(1-p_{RC}) \quad (4)$$

where $p_o(0)=p_{RC}$ and $p_i(0)= (1-p_{RC})/(N-1)$ for all $i\neq 0$ and $\alpha = -f_{oo}$. Excitation of the reaction center at various wavelengths should selectively excite different fractions of reaction centers. M_o could be measured using time resolved fluorescence providing the excitation is at wavelengths at which no accessory pigments are excited. (Pearlstein defines proximal pigments as all antenna pigments which have the lowest S_o- S_1 transition energy and therefore the excitons migrate directly to the RC's. All other pigments are accessory pigments.) At each excitation wavelength the fractional optical density, p_{RC}, due to RC absorbance must be determined [41]. A plot of M_o vs. $(1-p_{RC})$ should be linear and the slope gives τ_{FPT} (first passage time) from which a single site transfer time (SST) can be calculated. The estimate of the SST is only as good as the calculated Förster rate constants.

If it is assumed that all sites, individual antenna Chl's and RC's, are equally likely to be excited at t=0, then the rate equation is written [41]

$$M_o= [1+(F_D/F_T)(N-1)]k_p^{-1} + [1/qF_T - 1/qF_A][(N-1)^2/N] + \alpha N/F_A. \quad (5)$$

If only the RC is excited the rate equation becomes

$$M_o= [1+ (F_D/F_T)(N-1)]k_p^{-1}. \quad (6)$$

Owens et al. [4,5] took the approach outlined in Eqn. 5 to test the predictions of Pearlstein's model. Their experiments monitored the temporal characteristics of the fluorescence from PSI particles with varying sizes of antennas. For excitation

between 630 and 670 nm the fluorescence lifetime varied linearly with the size of the antenna. The analysis yielded a first passage time of ~20 psec with a SST of 0.21 psec. The excitation makes an average 2.4 reaction centervvisits before photoconversion and the excitation migration is diffusion limited.

Other researchers [26,31,49-54,59-63] have expanded the random walk model to test a variety of effects which might influence the efficiency of light harvesting. Seely [60] showed that spectral variety (spectral forms of Chl proteins that absorb at successively lower energy) can increase the trapping rate 4 to 5 times over that expected for a single wavelength absorbing Chl protein. This is achieved by enhancing the Förster overlap integral. Proper orientation of the electronic transition dipoles may introduce a similar factor of 4 to 5 times. It had already been suggested that if the longest wavelength absorbing form surrounds the RC, the trapping would be faster than if the surrounding Chls consist of a homogeneously absorbing protein complex [64,65]. This is the basis for the "funnel" model for the antenna.

Altmann and coworkers performed Monte Carlo calculations to study the effect of chlorophyll concentration and chlorophyll-trap ratio on the trapping rate in a two-dimensional random lattice [66]. They assumed the excitation undergoes a Förster type random walk migration. The calculated chlorophyll fluorescence lifetime agrees with in vivo results and is consistent with trapping upon first arrival at the trapping center.

Paillotin [52-53] used a Pauli master equation to describe the fluorescence quantum yield and fluorescence temporal decay of photosynthetic systems. Paillotin showed that the rate determining step in exciton capture is charge separation at the RC and that pigment heterogeneity promotes trapping at the RC (funnel effect).

Shipmann [61] using a Pauli master equation approach, incorporated Monte Carlo techniques to vary Chl position and orientation within regions determined by freeze-fractured photosynthetic membranes. Shipmann included variables such as Chl concentration, depth of trap, and the R_o Förster parameter to study antenna fluorescence lifetime, detrapping rates, and other factors. Two important conclusions are: 1) the fluorescence polarization is lost in <30 psec, and 2) the funnel effect is not required for efficient trapping of excitation at the RC since this would enhance both trapping and detrapping. He explains that the real purpose of absorption heterogeneity is to regulate the excitation flow from one photosystem to another within the thylakoid membrane [61]. Absorption and time resolved excitation and emission spectra of the core antenna complex of PSI show that the excitation in homogeneously distributed among all the spectral forms [5]. On this basis, Owens and coworkers [5] recently concluded that the funnel model does not apply to the core antenna protein of PSI.

Den Hollander et al. [16,17] expanded the master equation approach of Paillotin to discuss energy transfer, trapping, loss, and annihilation in a photosynthetic system. Their Monte Carlo calculations support the use of the random walk master equation model provided the densities of the excitations and RCs in a particular domain are small. They calculated the total fluorescence yields and the total fraction of RCs closed after the light pulse. These formulations were applied to data obtained by picosecond laser excitation of the purple bacteria Rhodospirillium rubrum and Rhodopseudomonas capsulata at various excitation intensities. The random walk approach is consistent with the data and yields a ratio of energy transfer between neighboring antenna molecules of $k_h = (1\text{-}2) \times 10^{12} s^{-1}$ for R. rubrum and $k_h = 4 \times 10^{11} s^{-1}$ for Rps. capsulata.

Kubzmauskas et al. [63] suggested that in some bacterial photosynthetic cases the approximation of infinitely high rate constant for trapping at the RC [41,60,62] is invalid and added a time limit of energy capture by the RCs. Their analysis incorporates a globular (subunit) structure of photosynthetic systems [63] into the master equation. In this approach the energy transfer within subunits is by coherent excitons and by incoherent excitons between subunits. Scherz and Parson [67] used a model involving strong (~ 730 cm^{-1}) exciton interactions within BChl dimers and weak (~ 35 cm^{-1}) between dimers to explain absorption and circular dichroism spectra obtained by Rafferty for the B800-850 complex of Rb. sphaeroides[68].

Other experimental evidence suggest that the Chls (BChls) in antenna systems are not arranged in a regular array lattice. The pigment-protein antenna complex for purple bacteria is postulated to be organized in large lakes which surround a network of B875 antenna that connect the RCs [69-71]. For the antenna pigments B800-850 of purple bacteria a "supramolecular" organization is proposed [71]. The Zuber model for B850 consist of "cyclic unit structure" of antenna BChl pairs in C_6 symmetry or possibly groups of 4 BChl in C_3 symmetry [72]. The model is consistent with the Scherz and Parsons model described earlier. The Kramer model [73] gives a basic structural unit consisting of four BChl 850, two BChl 800, and three carotenoid molecules. Although not perfect, the three models all give reasonable agreement with the available spectral data. Pearlstein [31] gives a current review.

The crystal structure of the antenna protein of P. aestuarii, a green photosynthetic bacteria, defines the basic structure to be a trimer of subunits [74,75]. Each subunit contains seven BChl a molecules. Analysis of the absorption and circular dichroism spectrum by Pearlstein [76] shows that the system possesses

strong excitonic coupling (~250 cm^{-1}) for BChl within the subunit. Recently, the time dependent absorption depolarization of the Q_x electronic transition in the P. aestuarii antenna protein complex at a time resolution of 1.5 psec was obtained [15]. Causgrove et al. [15] found that substantial residual polarization persist at long times. This is a consequence of the nonrandom orientation of the protein chromophores. Their interpretation is that excitons created within the tightly coupled BChls of a subunit hop (random walk) by a Förster mechanism between subunits.

Long time residual fluorescence polarization reported by Fetisova and coworkers for the green bacteria Chlorobium limicola and Chloroflexus aurantiacus, suggest that there is local ordering of the transition dipoles [6], possibly similar to P. aestuarii. "In this case the excitation energy transfer within BChl cantenna may be described as that between those clusters with parallel transition moments: each cluster may be considered as a single large 'molecule' which (as a whole) may serve as a donor or acceptor molecule in hopping-type excitation transfer" [6]. The proteins function to hold the BChl in precise alignment to optimize EET.

The three dimensional structure of the light harvesting chlorophyll a/bprotein complex determined at 30 A resolution using electron microscopy in negative stain gives a trimer of monomer Chls as the basic unit [77,78]. Pump-probe depolarization studies on the Chl a antenna complex of Photosystem I also gave a substantial residual polarization similar to that obtained on P. aestuarii [15]. This suggest that some form of local ordering also exist for this protein complex. The hop time between subunits is ~10 psec. This data is important since the crystal structure for green plant photosynthetic antenna systems has yet to be determined.

The discussion so far has centered on whether or not a subunit structure or regular array structure gives the best description of the photosynthetic antenna pigment-protein complexes. Final answer to this question awaits structure determination.

One final point to be mentioned before discussing multiphonon excitation energy transport theories, concerns the flow of excitation between PSI and PSII in green thylakoid membranes. The puddle model describes a PSU in which a given RC and its associated antenna system constitute a isolated PSU. Excitation created within a PSU cannot be transferred to another PSU. In the lake model [28], the RC resides in a lake of antenna pigment complexes and the excitations can migrate from RC to RC via antenna pigment complexes until it is captured or decays. The connected PSU model proposed by Joliot and Joliot [79] allows for partial connectivity between PSUs so that the excitation can migrate from a PSU with a closed RC to a neighboring PSU. The bipartate and tripartate models of Butler [80] attempt to account for energy distribution and fluorescence in PSII. Since these are kinetic models, the structural details of the antenna are not considered.

Recall that the analysis of Owens and coworkers [4,5] for the lifetime dependence of the fluorescence yielded a single site transfer time of ~ 0.2 psec at room temperature. NPHB experiments on C670 and PSI-200 antenna complexes indicate that the excitation depopulation lifetime at 1.6 K is ~300 psec. If these two values represent the same process, then nearly three orders of magnitude change occurs in going from room temperature down to 1.6 K. A tenfold decrease in EET between room temperature and 4 K is found for the B800-850 of Rb. sphaeroides using singlet-singlet annihilation techniques [19]. We turn now to multiphonon EET theory because the Förster rate equations does not explicitly describe the

temperature dependence of the rate. The temperature dependence is implied for the Förster expressions in the overlap integral, i.e. the overlap of the absorption spectrum of the acceptor and fluorescence spectrum of the donor changes as the temperature changes. Multiphonon EET theory also enjoys the freedom to address the subunit or regular array question since no assumptions about the antenna structure are made during the derivation.

Multiphonon excitation energy transport theory has its historical development in understanding non-radiative decay processes of ions and molecules in solids [56,81-86]. The classical limits (high temperature) were first developed to describe electron transfer reactions in solution at an electrode surface [87-89]. Semiclassical [90] and quantum calculations were applied by researchers [91-93] studying the temperature behavior of the DeVault and Chance cytochrome c reaction [94,95] and photosynthetic antenna systems [96]. Currently, the effort in this area has focussed on the nature of the excited states, and electron transfer processes in the reaction centers of purple photosynthetic bacteria [97-100].

The nonadiabatic microscopic rate equation for energy transport can be written in terms of the Fermi Golden Rule expression [101,102] :

$$W_{av\text{-}b} = \frac{2\pi}{\hbar} \sum_{w} |V_{av,bw}|^2 \, \delta(E_{bw} - E_{av}) \qquad (7)$$

Conceptually, this is written as a nonradiative decay process between a donor and acceptor. The summation is over all available system phonon and intramolecular modes. V is the matrix coupling element that includes the electron energy, lattice vibrations and the interaction between the electron and the lattice [84,85]. The δ

function insures the overlap of the initial and final states. This is the starting point for the classical and quantum mechanical treatment. We have assumed at this point that the microscopic rate $W_{av\text{-}b}$ for energy transport is slow compared to medium-induced vibrational relaxation (VR) and vibrational excitation [102]. The VR time scale for optical phonons have been experimentally determined with typical values being $\tau_{VR}^{-1} \sim 5x10^{-12}$ sec [103,104].

In the Condon approximation, the purely electronic coupling term can be separated from the vibrational term so that the matrix coupling element can be written

$$|V_{av,bw}|^2 = V^2 |<av|bw>|^2 \tag{8}$$

which upon substitution into Eqn. 7 yields

$$W_{av\text{-}b} = \frac{2\pi}{\hbar} V^2 \sum_w |<av|bw>|^2 \delta(E_{bw} - E_{av}). \tag{9}$$

We have assumed in the Condon approximation a separation of time scales so that the transition is vertical, i.e. the coordinates of the system do not change as quickly as the rate of the transfer process.

The macroscopic rate for energy transport can be written as the thermal average of the microscopic rates [95,102] so that

$$W_{a\text{-}b} = \sum_v p_v W_{av\text{-}b} \tag{10}$$

where the thermal occupation p_v is

$$p_v = \exp(-E_{av}/k_bT) / Z_1 \tag{11}$$

and

$$Z_1 = \sum_v \exp(-E_{av}/k_bT) \tag{12}$$

is the partition function of the donor manifold. The rate constant is then given as

$$W_{a\text{-}b} = \frac{2\pi}{\hbar} V^2 F \tag{13}$$

where F is the thermally averaged Franck-Condon factor

$$F = \sum_v \sum_w p_v |\langle av| bw\rangle|^2 \delta (E_{bw} - E_{av}). \tag{14}$$

It is this term that contains the thermal dependence.

The major problem in obtaining a tractable and physically understandable rate equation is performing the double summation in the F term. The problem is more difficult than presented in Eqns. 13 and 14 if one considers diagonal energy disorder [85,105,106]. Equation 14 was originally solved for the case in which all the modes available to the system have a common frequency by Huang and Rhys in 1950 [107]. A solution to the multi-frequency problem was first outlined by Kubo [83] and expanded by Kubo and Toyozawa [84]. Dogonadze et al. calculated the probability of the transitions between two multi-dimensional parabolic terms [108]. A simplified derivation of Kubo's result is given by DeVault [95] and Englman [81] and will not be given here.

The expressions written in terms of generating functions are

$$W_{a\text{-}b} = \frac{2\pi}{\hbar} V^2 \frac{1}{2\pi\hbar} \int_{-\infty}^{\infty} f(t) \exp(-i\Delta Et/\hbar)\, dt \tag{15}$$

with

$$f(t)=\exp\{-G + G_+(t) + G_-(t)\} \tag{16}$$

$$G_+(t)= \sum_k S_k (\bar{n}_k + 1) \exp(i\omega_k t) \tag{17}$$

$$G_-(t) = \sum_k S_k \bar{n}_k \exp(-i\omega_k t) \tag{18}$$

$$G = G_+(0) + G_-(0). \tag{19}$$

F(t) describes the time evolution of the system and the summation is over all k system modes. G_+ and G_- represent the absorption and emission , respectively, of one quantum of vibrational energy. G gives the initial condition of the system. S_k is the coupling strength (electron-phonon or electron-vibrational) and is generally written in reduced coordinates

$$S_k= \frac{1}{2} \Delta_k^2 \tag{20}$$

with Δ being the dimensionless nuclear coordinate [81,102]. $\bar{n}_k$ is the thermal occupation

$$\bar{n}_k = [\exp(\hbar\omega_k / k_b T)-1]^{-1} \tag{21}$$

with $\hbar\omega_k$ the mode frequency.

The term $\exp\{G_+(t) + G_-(t)\}$ can be written as

$$\exp\left\{\sum_k S_k[\bar{n}_k(\bar{n}_k+1)]^{1/2}\left[\left(\frac{\bar{n}_k+1}{\bar{n}_k}\right)^{1/2} \exp(i\omega_k t) + \left(\frac{\bar{n}_k}{\bar{n}_k+1}\right)^{1/2}\exp(-i\omega_k t)\right]\right\} \quad (22)$$

which can be expressed as [95,102]

$$\prod_k\left\{\sum_{m_k=-\infty}^{\infty}\left(\frac{\bar{n}_k+1}{\bar{n}_k}\right)^{m_k/2} I_{mk}\left\{2S_k[\bar{n}_k(\bar{n}_k+1)]\right\}^{1/2}\exp(m_k i\omega_k t)\right\} \quad (23)$$

where I_{m_k} is the modified Bessel function and m_k is the net change in quantum number for the oscillator mode k.

If we consider just the single mode case the rate equation becomes

$$W_{a\text{-}b}= \frac{2\pi}{\hbar} V^2\left(\frac{1}{2\pi\hbar}\right)\exp(-G)\ (2\bar{n}+1)\left(\frac{\bar{n}+1}{\bar{n}}\right)^{p/2} I_p\{2S[\bar{n}(\bar{n}+1)]\}^{1/2}\ x$$

$$\int_{-\infty}^{\infty} dt\ \exp\{i(p\omega-\Delta E/\hbar)t\} \quad (24)$$

which simplifies to

$$W_{a\text{-}b}= \frac{2\pi}{\hbar\omega} V^2 \exp[-S(2\bar{n}+1)]\left(\frac{\bar{n}+1}{\bar{n}}\right)^{p/2} I_p(2S[\bar{n}(\bar{n}+1)]^{1/2} \quad (25)$$

where $p=\Delta E/\hbar\omega$ with ΔE the energy difference between the donor and acceptor and $h\omega_s$ the frequency of the relevant mode. In this case, p is the number of quanta that will be necessary to account for the energy mismatch and thus assures energy overlap of the donor and acceptor states.

In the low temperature limit $\bar{n} \rightarrow 0$ so that

$$W_{a\text{-}b} = \left(\frac{2\pi}{h^2\omega_s}\right) V^2 \; e^{-S} \; \frac{S^p}{p!} \tag{26}$$

In the high temperature limit I_p can be expressed as a asymptotic expression [109]

$$I_p = (2\pi Z)^{-1/2} \exp\,(Z - p^2/2Z). \tag{27}$$

Substituting Eqn. 27 and

$$\frac{\bar{n}+1}{\bar{n}} = \exp(\hbar\omega/k_bT) \tag{28}$$

into Eqn. 25 with the appropriate high temperature limiting values [95]

$$2S[\bar{n}(\bar{n}+1)]^{1/2} - S(2\bar{n}+1) \rightarrow -S\hbar\omega/k_bT \tag{29}$$

and

$$2S[\bar{n}(\bar{n}+1)]^{1/2} \rightarrow 2Sk_bT/\hbar\omega \tag{30}$$

gives the exact expression

$$W = \frac{2\pi}{\hbar} V^2 \left(\frac{1}{4\pi S\hbar\omega k_b T}\right)^{1/2} \exp\text{-}\frac{(\Delta E - S\hbar\omega)^2}{4S\hbar\omega k_b T} \qquad (31)$$

for the single mode case. An alternate derivation of this result is given by Jortner [91]. If we let $\lambda = S\hbar\omega$ then the high temperature result is written as

$$W = \frac{2\pi}{\hbar} V^2 \left(\frac{1}{4\pi\lambda k_b T}\right)^{1/2} \exp\text{-}\frac{(\Delta E - \lambda)^2}{4\lambda k_b T} \qquad (32)$$

which is Marcus's result [88,89] with λ defined as the reorganization energy.

The multi-frequency equations can be calculated by carrying the summation terms of Eqns. 22 and 23. Both Jortner [91] and Sarai [92] have utilized a two mode formulation for inclusion of a low frequency protein mode (soft mode) and intramolecular vibration (hard mode) to explain the temperature dependence of the cytochrome c electron transfer reaction.

This section includes two papers that report results of NPHB on the light harvesting chlorophyll complex of PSI. The first paper gives results for the core antenna complex C670 in which a pseudo-phonon sideband hole and vibronic satellite holes are reported for the first time in a pigment-protein complex. The second paper reports a more in depth study done on the "native" PSI particle that contains its natural complement of Chl proteins. Multiphonon EET theory is used to account for the temperature dependence of the EET and explore possible structure models for the antenna complex.

ADDITIONAL RESULTS

It is interesting to consider how dispersion in phonon frequencies can alter the values of $\Delta E/hc$, V, and R obtained in Paper II. Table I and II present results for regular monomer array and subunit model, respectively, with delocalized phonons of frequencies $\hbar\omega_m = 10\ cm^{-1}$ and $30\ cm^{-1}$. Comparing Table I and II with Tables III and IV of Paper II reveals that a phonon frequency of $\hbar\omega_m = 10\ cm^{-1}$ gives results similar to that for $\hbar\omega_m \sim 20\ cm^{-1}$. In the regular array model $\Delta E/hc$ values for $\hbar\omega_m = 10 cm^{-1}$ are less than the corresponding values with $\hbar\omega_m \sim 20\ cm^{-1}$. Lower frequency phonons could serve to enhance EET in a regular monomer array model. Determination of the structure of the antenna protein would aid interpretation. The values of $\Delta E/hc$ for $\hbar\omega_m = 30\ cm^{-1}$ appear not to be physically reasonable since the inhomogeneous line width for Chl a is $300\ cm^{-1}$ (see Paper II) [110].

Noticeably absent from Table II are the values for S=0.1 for subunit model with $\hbar\omega_m = 30\ cm^{-1}$. It was not possible to account for the temperature dependence of EET using a value of S=0.1 (the best calculated value is τ_{DA}=37 psec). This behavior is hinted at for S=0.1 in Table I for $\hbar\omega_m = 30\ cm^{-1}$ and is common to all the calculations if S is made small enough. Remember that the corrected energy term is given by

$$\varepsilon = (\Delta E + S\hbar\omega_m)^2/4S\hbar\omega_m$$

with $S\hbar\omega_m$ being the reorganization strength. For the calculations presented here, if $\varepsilon \gtrsim 1000\ cm^{-1}$ then, it is not possible to account for the temperature dependence of

Table I. Regular monomer array model and delocalized phonons[a]

S	$\lvert\Delta E\rvert/hc$	$F_l \times 10^5/F_h \times 10^2$		$V(cm^{-1})/R(A)$	
		$\hbar\omega_m = 10\ cm^{-1}$			
0.1	32	8.8	6.4	11	35
0.2	39	8.7	6.2	12	35
0.5	54	6.8	5.0	13	34
		$\hbar\omega_m = 30\ cm^{-1}$			
0.1	148	0.009	0.007	584	10
0.2	135	1.1	0.85	54	21
0.5	171	2.8	0.022	34.3	25

[a] τ_{DA} (low temperature) = 750 psec, τ_{DA} (high temperature) = 1 psec. F_l and F_h are τ_{DA}^{-1}/A (see Eqns. 1, 2, 3 of Paper II) for low and high temperature, respectively.

Table II. Subunit model and delocalized phonons[a]

S	$\lvert\Delta E\rvert/hc$	$F_l \times 10^5/F_h \times 10^2$		$V(cm^{-1})/R(A)$	
		$\hbar\omega_m = 10\ cm^{-1}$			
0.1	40	0.38	3.1	5.2	46
0.2	47	0.59	4.1	4.5	48
0.5	64	0.47	3.8	4.7	47
		$\hbar\omega_m = 30\ cm^{-1}$			
0.2	180	0.007	0.06	67	20
0.5	210	0.094	0.71	18.8	30

[a] τ_{DA} (low temperature) = 300 psec, τ_{DA} (high temperature) = 10 psec. F_l and F_h are τ_{DA}^{-1}/A (see Eqns. 1, 2, 3 of Paper II) for low and high temperature, respectively.

the EET using S=0.1. Physically, this suggest that at some point the energy separation between chromophores (ΔE) overwhelms the ability of the phonons to mediate EET. This is similar to the problem of direct large energy transport between C670 and P700 discussed in Paper II. No Franck-Condon active excited state vibrational modes have been observed in the $\Delta E/hc$ range presented in Tables I and II. Phonons must therefore mediate EET with $\hbar\omega_m \sim 30\ cm^{-1}$ being an upper energy limit.

Spectral diffusion and dephasing processes in glasses manifest themselves in spectral hole burning by broadening the hole profile [111-113]. The excitation depopulation lifetime T_1 is calculated by

$$T_1 = \frac{1}{\pi \Delta\nu_{hole}}$$

if spectral diffusion and dephasing processes (T_2^* processes) are ignored. In this case, excitation depopulation lifetimes calculated from $\Delta\nu_{hole}$ are shorter than the actual value. For this reason we report a lower limit of $\tau_{DA} = 300$ psec.

The maximum rate for EET can be calculated by setting $-\Delta E = S\hbar\omega_m$ [89]. The rate constant at low temperature is readily calculated from

$$\tau_{DA}^{-1}(\text{low T}) = \tau_{DA}^{-1}(\text{high T}) \times \frac{e^{-S} S^p / p!}{(\hbar\omega_m / 4\pi SkT)^{1/2}}$$

with $p = \Delta E/\hbar\omega_m = S$. Table III gives τ_{DA} (low T) and $\Delta\nu_{hole}$ for delocalized phonons within the regular monomer array and subunit model for the antenna. τ_{DA} (low T) is much shorter than observed experimentally. The hole profiles are not

Table III. Optimum Low Temperature Transfer Time

S	τ_{DA} (psec)	$\Delta\nu_{hole}$ (cm^{-1})
	Regular Array[a]	
0.1	0.38	28
0.2	0.32	24
	Subunit Model[b]	
0.1	3.8	1.4
0.2	3.2	1.7

[a] τ_{DA} (high T)= 1 psec.

[b] τ_{AD} (high T)= 10 psec.

dominated by the broadening which would have been suspected if the calculated τ_{DA} was greater than 300 psec. For example, if the maximum rate for EET was ~600 psec ($\Delta\nu_{hole} = 0.02$ cm^{-1}), then since the experimental holewidths are ~ 0.03 cm^{-1} ($\tau_{DA} = 300$ psec) other processes such as spectral diffusion and dephasing that broaden the holes could be dominating the relaxation process being measured. Further experiments are needed, however, to define the influence of spectral diffusion and dephasing in the antenna complex. It is not necessarily to be expected that the rate of EET is at its maximum because this could lead to a inefficient bottleneck of the excitation waiting to be photoconverted at the RC.

The Stark effect is a general term used to label the influence of electric fields on atomic or molecular spectroscopy. A molecule placed in an electric field m=ν+ αF, undergoes a change in potential energy caused by work done on the dipole. The potential change, V, is [114]

$$V = -\int_0^F \vec{m}\, d\vec{F} = -\vec{\mu}\cdot\vec{F} - \frac{1}{2}\vec{F}\cdot\vec{\alpha}\cdot\vec{F}$$

where μ is the permanent dipole moment and α is the polarizibility tensor. If θ is the angle between the dipole and electric field, then

$$V(F) = -\Delta\mu F\cos\theta - 1/2\ \Delta\alpha F^2$$

with $\Delta\mu = \mu_e - \mu_g$ is the difference of the electric dipole moment of the excited (e) and ground (g) state and $\Delta\alpha$ the polarizibility difference. F= fE with E being the externally applied field and $f=(\varepsilon_o+2)/3$, the Lorentz local-field correction for a dielectric constant ε_o. The field induced changes allows one to probe the molecular

dipole and polarizibility and intermolecular interactions. For example, Stark effect can be used to split the n-fold orientation degeneracy of impurities doped into molecular crystals by altering the field along a particular molecular axis. The observed effect is a splitting of the electronic transition (splitting of the spectral line) with an energy difference

$$\Delta E = 2F\Delta\mu\,|\cos\theta|.$$

For excitonic states, Stark effect can alter the resonance between states. For a review of Stark effect on molecular crystals see ref. 114.

The Stark effect is easily studied in molecular crystals since the linewidths at low T are narrow. It is more difficult in amorphous materials since the linewidth is large (several hundred cm^{-1}), however, site selective spectroscopies, in particular spectral hole burning, produce narrow features which allows us to investigate Stark effect in these systems. The Stark effect on spectral holes is not as straight forward as for crystals. The hole shape calculation must account for the shifting of molecular electronic transitions in and out of resonance with the burn frequency. The calculations must also include an integration over all dipole orientation angles since the dipoles are not aligned as in a molecular crystal [115,116].

The Stark effect results in a shift in the transition frequency which is displayed in spectral hole burning by a broadening [$E_{laser} \perp E_{field}$] or splitting [$E_{laser} \parallel E_{field}$] of the hole profile for a parallel dipole moment and transition moment [115,116]. The frequency shift is given by

$$h\Delta\nu = -f\Delta\mu\cdot F - \frac{1}{2} f^2\, F\cdot\Delta\alpha\cdot F$$

where E is the external field given in V/d, f is the Lorentz field factor, $\Delta\mu$ is the change in dipole moment and $\Delta\alpha$ is the polarizability of the molecule. Second order effects have never been observed so the frequency shift simplifies to

$$h\Delta\nu = - f\,\Delta\mu\cdot F.$$

The slope of the plot of holewidth (broadening) or hole splitting versus the electric field is used to calculate $\Delta\mu$ in the ground to excited state electronic transition.

The Stark effect absorption spectra for the RC of Rps. viridis demonstrates a large change in the dipole moment between the ground and excited state (~9 D) indicating substantial charge transfer character for the primary electron donor [117]. This is consistent with the hole burned spectra for the RCs of PSU which shows a strong electron-phonon coupling [118,119]. Such charge transfer characteristic would have important consequence in discussing EET in antenna systems. Although no spectral evidence for charge transfer in the antenna exist, Stark effect spectroscopy provides a simple check.

Stark effect is not observed for the Chl in the core antenna complex of PSI. The uncertainty in the holewidths is ~0.002 cm^{-1} and the maximum applied E field was ~750 V/cm. A value for the dielectric constant for the protein complex is not available and will be taken as that for polymers, ε_o=3.0 [117]. The calculation gives $\Delta\mu$<0.1 D for the core antenna Chl. The change in the dipole is small consistent with weak linear electron-phonon coupling and electron-vibrational coupling. This implies that the excited state potential surface is not greatly perturbed from the

ground state. The measured $\Delta\mu$ for Zn-tetrobenzoporphin in poly(vinyl butyral) is ~0.2D and for isobacteriochlorin in n-octane $\Delta\mu$~1.6D [118,119].

No evidence for spontaneous hole refilling (SPHF) or laser induced hole refilling (LIHF) has been observed. This observation also removes global spectral diffusion and anti-hole reversion through external two level systems, processes speculated to be active in ionic dyes doped into polymers [111,113], as active processes in the antenna. More data such as hole growth and hole refilling studies are needed before a complete picture can be forwarded.

This work demonstrates that spectral hole burning is an important new tool for studying dynamical processes in protein bound complexes. A number of interesting new results have been presented to answer important questions, but, a number of new questions have also arisen. A more complete understanding of EET in the antenna system of PSI awaits more thorough investigation of protein effects on hole burning and structure determination.

REFERENCES

1. Lotshaw, W. T.; Alberte, R. S.; Fleming, G. R. Biochim. Biophys. Acta 1982, 682, 75.

2. Gulotty, R. J.; Fleming, G. R.; Alberte, R. S. Biochim. Biophys. Acta 1982, 682, 322.

3. Gulotty, R. J.; Mets, L.; Alberte, R. S.; Fleming, G. R. Photochem. Photobiol. 1985, 41, 487.

4. Owens, T. G.; Webb, S. P.; Mets, L.; Alberte, R. S.; Fleming, G. R. Proc. Natl. Acad. Sci. U.S.A. 1987, 84, 1532.

5. Owens, T. G.; Webb, S. P.; Mets, L.; Fleming G. R. Biophys. J. 1988, 53, 733.

6. Fetisova, Z. G.; Freiberg, A. M.; Timpmann, K. E. Nature 1988, 334, 633.

7. Searle, G. F. W.; Tamkivi, R.; van Hoek, A. ; Schaafsma, T. J. J. Chem. Soc., Faraday Trans. 2 1988, 84, 315.

8. Mimuro, M.; Tamai, N.; Yamazaki, I. FEBS Lett. 1987, 213, 119.

9. Gillbro, T.; Sundström, V.; Sandström, Å.; Spangfort, M.; Andersson, B. FEBS Lett. 1985, 193, 267.

10. Avarmaa, R. A.; Kochubey, S. M.; Tamkivi, R. P. FEBS Lett. 1979, 102, 139.

11. Avarmaa, R.; Renge, I.; Mauring, K. FEBS Lett. 1984, 167, 186.

12. Sundström, V.; van Grondelle, R.; Bergström. H.: Åkesson, E.; Gillbro, T. Biochim. Biophys. Acta 1986, 851, 531.

13. Bergström, H.; Sundström, V.; van Grondelle, R.; Åkesson, E.; Gillbro, T. Biochim. Biophys. Acta 1980, 852, 279.

14. Causgrove, T.; Yang, S.; Struve, W.S. J. Phys. Chem. 1988, 92, 6121.

15. Causgrove, T.; Yang, S.; Struve, W.S. J. Phys. Chem. 1988, 92, 6790.

16. Den Hollander, W. T. F.; Bakker, J. G. C.; van Grondelle, R. Biochim. Biophys. Acta 1983, 725, 492.

17. Bakker, J. G. C.; van Grondelle, R.; Den Hollander, W. T. F. Biochim. Biophys. Acta 1983, 725, 508.

18. Dobek, A.; Deprez, J.; Geacintov, N. E.; Paillotin, G.; Breton, J. Biochim. Biophys. Acta 1985, 806, 81.

19. Vos, M.; van Grondelle, R.; van der Kooij, F. W.; van de Poll, D.; Amesz, J.; Duysens, L. N. M. Biochim. Biophys. Acta 1986, 850, 501.

20. Vos, M.; van Dorssen, R. J.; Amesz, J.; van Grondelle, R.; Hunter, C. N. Biochim. Biophys. Acta 1988, 933, 132.

21. Renge, I.; Mauring, K.; Avarmaa, R. Biochim. Biophys. Acta 1984, 766, 501.

22. Renge, I.; Mauring, K.; Vladkova, R. Biochim. Biophys. Acta 1988, 935, 333.

23. Mauring, K.; Renge, I.; Avarmaa, R. FEBS Lett. 1987, 223, 165.

24. Gillie, J. K.; Hayes, J. M.; Small, G. J.; Golbeck, J. H. J. Phys. Chem. 1987, 91, 5524.

25. Gillie, J. K.; Small, G. J.; Golbeck, J. H. J. Phys. Chem. 1989, 93, 1620.

26. Knox, R. S. In Primary Processes of Photosynthesis; Barber, J., Ed.; Elsevier: Amsterdam, 1977, p 56.

27. Knox, R. S. In Photosynthetic Membranes and Light Harvesting Systems; Staehelin, L.; Arntzen, C., Eds.; Springer-Verlag: Berlin, 1986, p 286.

28. Geacintov, N. E.; Breton, J. CRC Crit. Rev. Plant. Sci. 1987, 5, 1.

29. van Grondelle, R. Biochim. Biophys. Acta 1985, 811, 147.

30. Holzwarth, A. R. In The Light Reactions; Barber, J., Ed.; Elsevier: Amsterdam, 1987, p 95.

31. Pearlstein, R. M. In Photosynthesis; Amesz, J. Ed.; Elsevier: Amsterdam, 1987, p 299.

32. Franck, J.; Teller, E. J. Chem. Phys. 1938, 6, 861.

33. Frenkel, J. Phys. Rev. 1931, 37, 17; Phys. Rev. 1931, 37, 1276.

34. Peierls, R. Ann. d. Physik 1932, 13, 905.

35. Emerson, R.; Arnold, W. A. J. Gen. Physiol. 1932, 15, 391.

36. Emerson, R.; Arnold, W. A. J. Gen. Physiol. 1932, 15, 191.

37. Gaffron, H.; Wohl, K. Naturwissenschaften 1936, 24, 81; Naturwissenschaften 1936, 24, 103.

38. Govindjee; Govindjee, R. In Bioenergetics of Photosynthesis; Govindjee, Ed.; Academic; New York, 1975, p 2.

39. Robinson, G. W. Brookhaven Symposia in Biology 1967, 19, 16.

40. Bay, Z.; Pearlstein, R. M. Proc. Natl. Acad. Sci. U.S.A. 1963, 50, 1071.

41. Pearlstein, R. M. Photochem. Photobiol. 1982, 35, 835.

42. Harris, C. B.; Zwemer, D. A. Ann. Rev. Phys. Chem. 1978, 29, 473.

43. Munn, R. W.; Silbey, R. Mol. Cryst. Liq. Cryst. 1980, 57, 131.

44. Fayer, M. D.; Harris, C. B. Phys. Rev. B 1974, 9, 748; Phys. Rev. B 1974, 10, 1784.

45. Stevenson, S. H.; Connolly, M. A.; Small, G. J. Chem. Phys. 1988, 128, 157.

46. Fayer, M. D.; Harris, C. B. Chem. Phys. Lett. 1974, 25, 149.

47. Johnson, S. G.; Small G. J. Chem. Phys. Lett. 1989, 155, 371.

48. Johnson, C. K.; Small, G. J. In Excited States; Lim, E. C., Ed.; Academic: New York, 1982; Vol. 6, p 97.

49. Kenkre, V. M.; Knox, R. S. Phys. Rev. B 1974, 9, 5279.

50. Kenkre, V. M.; Knox, R. S. Phys. Rev. Lett. 1974, 33, 803.58.

51. Kenkre, V. M.; Knox, R. S. J. Lumin. 1976, 12, 187.

52. Paillotin, G. J. Theor. Biol. 1972, 36, 223.

53. Paillotin, G. J. Theor. Biol. 1976, 58, 219.

54. Paillotin, G.; Swenberg, C. E.; Breton, J.; Geacintov, N. E. Biophys. J. 1979, 25, 513.

55. Paillotin, G. In Advances in Photosynthesis Research; Sybesma, C., Ed.; Martinus Nijhoff/Dr. W. Junk: The Netherlands, 1984, Vol. 1, p 5.

56. Pearlstein, R. M. In Advances in Photosynthesis Research; Sybesma, C., Ed.; Martinus Nijhoff/Dr. W. Junk: The Netherlands, 1984, Vol. 1, p 13.

57. Förster, T. Discuss. Faraday Soc. 1959, 27, 7.

58. Borisov, A. Y. In The Photosynthetic Bacteria; Clayton, R. K., Sistrom, W. R., Ed.; Plenum; New York, 1978, p 323.

59. Montroll, E. W. J. Math. Phys. 1969, 10, 753.

60. Seely, G. R. J. Theor. Biol. 1973, 40, 173; J. Theor. Biol. 1973, 40, 189.

61. Shipmann, L. L. Photochem. Photobiol. 1980, 31, 157.

62. Knox, R. S. J. Theor. Biol. 1968, 21, 244.

63. Kudzmaukas, S.; Valkunas, L.; Borisov, A. Y. J. Theor. Biol. 1983, 105, 13.

64. Borisov, A. Y. Biofizika 1967, 12, 630.

65. Borisov, A. Y.; Fetisova, Z. G. Molekulyarnaya Biologia 1971, 5, 509.

66. Altmann, J. A.; Beddard, G. S.; Porter, G. Chem. Phys. Lett. 1978, 58, 54.

67. Scherz, A.; Parson, W. Photosynthesis Research 1986, 9, 21.

68. Rafferty, C. N.; Bolt, J.; Sauer, K.; Clayton, R. K. Proc. Natl. Acad. Sci. U.S.A. 1979, 76, 4429.

69. Monger, T. G.; Parson, W. W. Biochim. Biophys. Acta 1977, 460, 393.

70. Cogdell, R. J.; Thornber, J. P. FEBS Lett. 1980, 122, 1.

71. Loach, P. A.; Parkes, P. S.; Miller, J. F.; Hinchigeri, S.; Callahan, P. M. In Molecular Biology of the Photosynthetic Apparatus; Steinbeck, K. E., Ed.; Cold Spring Harbor Laboratory: New York, 1985, p 197.

72. Zuber, H.; Sidler, W.; Füglistaller, P.; Brunisholz, R.; Theiler, R. In Molecular Biology of the Photosynthetic Apparatus; Steinbeck, K. E., Ed.; Cold Spring Harbor Laboratory: New York, 1985, p 183.

73. Kramer, H. J. M.; Grondelle, R.; Hunter, C. N.; Westerhuis, W. H. J.; Amesz, J. Biochim. Biophys. Acta 1984, 765, 156.

74. Matthews, B. W.; Fenna, R. E. Acc. Chem. Res. 1980, 13, 309.

75. Tronrud, R. E.; Schmid, M. E.; Matthews, B. W. J. Mol. Biol. 1986, 188, 443.

76. Pearlstein, R. M.; Hemenger, R. P. Proc. Natl. Acad. Sci. U.S.A 1978, 75, 4920.

77. Li, J. Proc. Natl. Acad. Sci. U.S.A. 1985, 82, 386.

78. Kuhlbrandt, W. Nature 1984, 307, 478.

79. Joliot, A.; Joliot, P. C. R. Acad. Sci. 1964, 258, 4622.

80. Butler, W. L. Ann. Rev. Plant Physiol. 1978, 29, 345.

81. Englman, R. Non-Radiative Decay of Ions and Molecules in Solids; North Holland: Amsterdam, 1979.

82. Dexter, D. L. J. Chem. Phys. 1953, 21, 836.

83. Kubo, R. Phys. Rev. 1952, 86, 929.

84. Kubo, R.; Toyozawa, Y. Progress of Theor. Phys. 1955, 13, 160.

85. Soules, T. F.; Duke, C. B. Phys. Rev B 1971, 3, 262.

86. Duke, C. B. Mol. Cryst. Liq. Cryst. 1979, 50, 63.

87. Marcus, R. A. J. Chem. Phys. 1956, 24, 966.

88. Marcus, R. A. Annu. Rev. Phys. Chem. 1964, 15, 155.

89. Marcus, R. A. Faraday Discuss. Chem. Soc. 1982, 74, 7.

90. Hopfield J. J. Proc. Natl. Acad. Sci. U.S.A. 1974, 71, 3640.

91. Jortner, J. J. Chem. Phys. 1976, 64, 4860.

92. Sarai, A. Chem. Phys. Lett. 1979, 63, 360.

93. Tunneling in Biological Systems; Chance, B.; DeVault, D. C.; Frauenfelder, H.; Marcus, R. A.; Schieffer, J. R.; Sutin, N., Eds.: Academic: New York, 1979.

94. DeVault, D.; Chance, B. Biophys. J. 1966, 6, 825.

95. Devault, D. Quar. Rev. Biophysics 1980, 13, 387.

96. Yomosa, S. J. Phys. Soc. Japan 1978, 45, 967.

97. Jortner, J. Biochim. Biophys. Acta 1980, 594, 193.

98. Jortner, J. J. Phys. Chem. 1986, 90, 3795.

99. Marcus, R. A.; Sutin, N. Biochim. Biophys. Acta 1985, 811, 265.

100. Marcus, R. A. In Supramolecular Photochemistry; Balzani, V. Ed.; D. Reidel: New York, 1987, p 45.

101. Levich, V. G. In Physical Chemistry: An Advanced Treatise; Eyring, H.; Henderson, D.; Jost, W., Eds.; Academic: New York, Vol. 9B,1970.

102. Jortner, J. J. Am. Chem. Soc. 1980, 102, 6676.

103. Laubereau, A.; Von Der Linde, D.; Kaiser, W. Phys. Rev. Lett. 1971, 27, 802.

104. Laubereau, A.; Wochner, G.; Kaiser, W. Opt. Commun. 1975, 14, 175.

105. Holstein, T.; Lyo, S. K.; Orbach, T. Comments Solid State Phys. 1978, 8, 119.

106. Holstein, T.; Lyo, S. K.; Orbach, R. J. Lumin. 1979, 18/19, 634.

107. Huang, K.; Rhys, A. Proc. R. Soc. Lond. A 1950, 204, 406.

108. Dogonadze, R. R.; Kuznetsov, A. M.; Vorotyntsev, M. A. Phys. Stat. Sol. B 1972, 54, 125.

109. Watson, G. N. A Treatise on the Theory of Bessel Functions; University Press: New York, 1945.

110. Gillie, J. K.; Fearey, B. L.; Hayes, J. M.; Small, G. J.; Golbeck, J. H. Chem. Phys. Lett. 1987, 134, 316.

111. Jankowiak, R.; Small, G. J. Science 1987, 237, 618.

112. Friedrich, J.; Haarer, D. In Optical Spectroscopy of Glasses; Zschokke, I., Ed.; Reidel: Dordecht, Netherlands, 1986, 149.

113. Hayes, J. M.; Jankowiak, R.; Small, G. J. In Persistent Spectral Hole-Burning: Science and Application; Moener, W. E., Ed.; Springer-Verlag: West Berlin, 1988, 153.

114. Hochstrasser. R. M. Acc. Chem. Res. 1973, 6, 263.126.

115. Meixmer, A. J.; Renn, A.; Bucher, S.E.; Wild, U. P. J. Phys. Chem. 1986, 90, 6777.

116. Maier, M. Appl. Phys. B 1986, 41, 73.

117. Lockhart, D. J.; Boxer, S. G. Biochemistry 1987, 26, 664.125.

118. Hayes, J. M.; Small, G. J. J. Phys. Chem. 1986, 90, 4928.

119. Hayes, J. M. ; Gillie, J. K.; Tang, D.; Small, G. J. Biochim. Biophys. Acta 1988, 932, 287.

118. Kador, L.; Haarer, D.; Personov, R. J. Chem. Phys. 1987, 86, 10.

119. Kador, L.; Personov, R. Richter, W.; Sesselmann, Th.; Haarer, D. Polymer J. 1987, 19, 61.

ACKNOWLEDGMENTS

This dissertation is dedicated to the loving memory of my brother Alan Stephen Gillie, May 4, 1963 - December 20, 1985. Few events in one's life can be so painful yet so influencing. We will never have the chance now to collaborate in a scientific endeavor as we once dreamed. I miss his companionship, his jokes and animated gestures, but mostly I miss his love. This dissertation is also dedicated to the memory of my grandmother Ethel Gillie whom I wish could share my joy of graduating.

I wish to thank my parents for their encouragement through the years, their love and support, and most of all the patience to answer all the questions three curious boys can ask. I also wish to thank my older brother Michael for all the fun and friendship that only an older brother can provide.

I also express thanks to everyone who has played an important part in my scientific development. I am most grateful to Dr. Gerald J. Small who provided needed guidance while allowing me the freedom to pursue the aspects of this project I found most interesting. His patience and thoughtful discussions were very important. I also thank Dr. John Hayes and Dr. Ryszard Jankowiak for their many discussions through the years. I cannot imagine two better coworkers. To my friends in Dr. Small's group, thanks for all the help and good times. The practical jokes have always been enjoyable.

Finally, I thank my other friends who made my stay at ISU enjoyable. I especially thank my girlfriend, Patrice Christensen, for the good times, companionship and love of the last two years.

This work was performed at Ames Laboratory under contract No. W-7405-eng-82 with the U. S. Department of Energy. The United States government has assigned the DOE Report number IS-T 1403 to this thesis.